

## Zircon U-Pb and Hf isotopic constraints on the genesis of a post-kinematic S-type Variscan tin granite: the Logrosán cupola (Central Iberian Zone)

E. Chicharro<sup>1,2\*</sup>, C. Villaseca<sup>2,3</sup>, P. Valverde-Vaquero<sup>4</sup>, E. Belousova<sup>5</sup>, J.A. López-García<sup>1</sup>

<sup>1</sup>Dpt. Cristalografía y Mineralogía, Facultad Ciencias Geológicas, Universidad Complutense de Madrid, 28040 Madrid, Spain.

<sup>2</sup>Instituto de Geociencias (UCM, CSIC), c. José Antonio Novais, 12, 28040 Madrid, Spain

<sup>3</sup>Dpt. Petrología y Geoquímica, Facultad Ciencias Geológicas, Universidad Complutense de Madrid, 28040 Madrid, Spain.

<sup>4</sup>Instituto Geológico y Minero de España (IGME), Madrid, Spain.

<sup>5</sup>Dpt. Earth and Planetary Sciences, GEMOC, Macquarie University, Sydney, NSW 2109, Australia.

e-mail addresses: evachicharro@ucm.es (E.C., \*corresponding author); granito@ucm.es (C.V.); p.valverde@igme.es (P.V.-V.); ebelouso@els.mq.edu.au (E.B.); jangel@geo.ucm.es (J.A.L-G.)

Received: 10 January 2014 / Accepted: 10 June 2014 / Available online: 30 October 2014

### Abstract

The Variscan Orogeny produced widespread granites along the European Variscan belt. In relation to crustal thickening, post-collisional multiple Sn-bearing highly fractionated S-type leucogranites were emplaced. The Logrosán granite represents one of those granitic bodies and is the focus of this study. The Logrosán granite is located in the Central Extremadura Batholith, within the Central Iberian Zone (CIZ) and was emplaced during post kinematic stages of the Variscan Orogeny at ca. 308 Ma, as determined by combined U-Pb ID-TIMS and LA-ICPMS geochronology. The granitic body intruded the metasedimentary Schist Greywacke Complex (SGC) of Neoproterozoic age. A moderately evolved medium- to coarse-grained two mica leucogranite (Main Unit) and several highly evolved aplitic or microporphyritic units (Evolved Units) have been distinguished based on their petrography and whole rock geochemistry. Initial  $^{87}\text{Sr}/^{86}\text{Sr}$  ratios vary from 0.7125 to 0.7286, whereas initial  $\epsilon\text{Nd}$  shows a restricted range from -4.3 to -4.0 and  $\epsilon\text{Hf}_{(0)}$  ranges from +5.7 to -10.5 for Variscan-age zircons. Inherited zircons exhibit mostly Neoproterozoic ages and juvenile Hf-isotope composition ( $\epsilon\text{Hf}$  up to +14.7) analogous to zircons from the SGC metasediments. The available geological, geochronological, geochemical and isotopic data allow us to propose partial melting of heterogeneous Neoproterozoic metasediments, similar to the outcropping SGC materials for the genesis of the Logrosán granite.

**Keywords:** Sr-Nd isotopes, zircon Hf isotopes, fractionated S-type granites, tin granites, Iberian Variscan Belt

### Resumen

La orogenia Varisca produjo una gran cantidad de granitos a lo largo del Cinturón Varisco Europeo. En relación con el engrosamiento cortical se emplazaron tardíamente granitos de tipo-S, muy fraccionados y ricos en Sn. El presente estudio se centra en uno de esos cuerpos graníticos, el granito de Logrosán. El plutón de Logrosán forma parte del Batolito de Extremadura Central (BEC), en la Zona Centroibérica (ZCI), y se emplazó durante las etapas tardías de la orogenia Varisca, a los ca. 308 Ma, según los datos combinados de geocronología de U-Pb por ID-TIMS y por LA-ICPMS. El cuerpo granítico intruyó los metasedimentos del Complejo Esquistoso Grauváquico (CEG) de edad fundamentalmente Neoproterozoica. En el plutón se distinguen, de acuerdo a la petrografía y a la geoquímica de roca total, un leucogranito de dos micas de tamaño de grano medio-grosso moderadamente evolucionado (Main Unit) y varias unidades aplíticas o microporfídicas altamente evolucionadas (Evolved Units). Las relaciones isotópicas iniciales de  $^{87}\text{Sr}/^{86}\text{Sr}$  varían de 0.7125 a 0.7286, mientras que el  $\epsilon\text{Nd}$  inicial muestra un rango restringido de -4.3 a -4.0 y el  $\epsilon\text{Hf}_{(0)}$  en circones variscos oscila de +5.7 a -10.5. Los circones heredados del granito de Logrosán muestran edades principalmente Neoproterozoicas y composiciones isotópicas de Hf juveniles ( $\epsilon\text{Hf} > +14.7$ ), análogas a las encontradas en los circones del CEG. Los datos geológicos, geoquímicos, geocronológicos e isotópicos de los que se dispone sugieren que el granito de Logrosán se originó por la fusión parcial de materiales metasedimentarios Neoproterozoicos similares a los del CEG.

**Palabras clave:** isótopos de Sr-Nd, isótopos de Hf en circón, granitos fraccionados de tipo S, granitos estanníferos, Cinturón Varisco Ibérico

## 1. Introduction

The Variscan Orogeny generated a huge volume of granitic melts. The Iberian Belt shows the largest concentration of felsic magmatism within western Europe, mainly in its inner parts. The Central Iberian Zone (CIZ) is composed by vast granite batholiths drawing sub-concordant major linear arrays (Fig. 1a) (e.g., López Plaza and Martínez Catalán, 1987). During the last two decades, U-Pb zircon geochronology has been applied to different granite plutons of these batholiths (e.g., Fernández-Suárez *et al.*, 2000; Dias *et al.*, 1998). Much more recently, combined U-Pb and Lu-Hf isotope systematics on zircon grains have been used to identify source components and to constrain the age of heterogeneous inheritances incorporated in the granite genesis. This integrated isotope information contributed significantly to the discussions on the origin of the Central Iberian granites (e.g., Villaseca *et al.*, 2012; Teixera *et al.*, 2011).

In this work we have studied a small felsic cupola of the southern part of the CIZ related to two types of mineralizations: i) an intra-granitic D cassiterite-bearing vein-complex, usually related to greisen-like alteration, ii) an exo-granitic P-rich ore of hydrothermal apatite (dahllite)-quartz veins (Vindel *et al.*, 2014; Locutura *et al.*, 2007). Other batholiths of this southern part of the CIZ have been dated by U-Pb zircon geochronology (Castelo Branco: Antunes *et al.*, 2008; Cabeza de Araya: Gutiérrez-Alonso *et al.*, 2011; Nisa-Alburquerque: Solá *et al.*, 2009; Montes de Toledo: Orejana *et al.*, 2012), but none of them have been studied by the combined U-Pb and Hf-isotope approach. Therefore, we have used a combination of zircon U-Pb CA-ID-TIMS and LA-ICP-MS geochronology to better constrain the age of the granite emplacement and of the inherited zircons.

## 2. Geological Setting

The Logrosán pluton is located in the Central Iberian Zone (CIZ) (Julivert *et al.*, 1972) of the Iberian Massif, at the southeast of the Cáceres province (Spain) (Fig. 1a). Large volumes of granitoids were emplaced during the post-collisional stage of the Variscan Orogeny, mostly late- to post-kinematically to the D<sub>3</sub> event (e.g., Dias *et al.*, 1998). The Logrosán granite is one of the post-kinematic bodies of the Central Extremadura Batholith (Castro, 1985) that intrudes into epizonal domains of the CIZ. The Logrosán granite is a small body that represents a typical felsic cupola related to complex hydrothermal mineralizations. Tin-tungsten deposits associated with granites in the Iberian Variscan Belt occur mainly in the Central Iberian Zone and constitute one of the most important Sn-W metallogenic provinces of the European Variscan Belt. Sn mineralization befalls as cassiterite-quartz stockwork and greisen type ore in the Logrosán granite. The Logrosán granite intruded the Neoproterozoic metasedimentary series of the Schist Greywacke Complex

(SGC) which is characterized in this area by a monotonous decimetric to centimetric alternation of greywackes and shales with minor presence of sandstones and conglomerates (Fig. 1b). A Variscan low-grade regional metamorphism (Chl-Bt zone) has affected these Neoproterozoic country rocks. Moreover, the emplacement of the Logrosán granite has produced a superimposed contact metamorphism characterized by an inner biotite-tourmaline hornfels zone, an intermediate zone of micaceous spotted slates, and a transition zone of recrystallized slates and some metaquartzite levels (Fig. 1c).

The dominant regional structural pattern in the area is Variscan in age. The main Variscan deformation phases defined in the CIZ are also recognized in the area. D1 and D2 deformation phases correspond to the collisional stage of the Variscan orogeny and the crustal thickening which is associated with partial melting and a restricted production of peraluminous granitoids (Dias *et al.*, 1998). The metasediments were folded during the first Variscan phase (D1) which started at 360 Ma in the CIZ (Ábalos *et al.*, 2002; Dallmeyer *et al.*, 1997). D1 compressional structures are constituted by large, subvertical folds oriented N100/110E and associated with a schistosity (S1) parallel or transverse to the axial plane (Quesada *et al.*, 1987). The emplacement of the Logrosán granite produced some deviations in the S1 orientation until it reaches E-W directions. A greenschist facies metamorphic grade is reached in the area. The second deformation phase occurred during Lower-Middle Carboniferous (330-310 Ma) (Martínez Catalán, 2011; and references therein). D2 event has an extensional character (Díez Balda *et al.*, 1995) and it is characterized by recumbent folds associated with dextral shear zones (N40-N60) with an axial plane crenulation cleavage or schistosity (S2). The S2 schistosity is occasionally recognized in the studied area. The D3 phase took place between 320 and 312 Ma (López-Moro *et al.*, 2012; Valle Aguado *et al.*, 2005; Dias *et al.*, 2002) and constitutes the last ductile regional deformation phase. It is characterized by the generation of open to tight vertical folds with subhorizontal axes and subvertical shear zones with sinistral (NW-SE) or dextral (NE-SW) wrench movement (Dias *et al.*, 1998). In the studied area shear zones are dextral with an ENE-WSW direction. On a regional scale, it has been assumed that such D3 structures were developed in a distensive context related to gravitational collapse and generalized extension across the belt (Díez Balda *et al.*, 1995; Rodríguez-Pevida *et al.*, 1990). Granite plutons, such as the Logrosán granite, were intruded later or post-kinematically to the D3 phase. Finally, the D4 fragile deformation phase corresponds to extension tectonics that took place from Middle Carboniferous to Permian times (Dias *et al.*, 1998). In the studied area, D4 structures are characterized by the reactivation of old D3 faults in the opposite direction. These faults provided active channels for the flow of mineralized fluids and are almost certainly related to the tin ore vein system of the Logrosán granite.

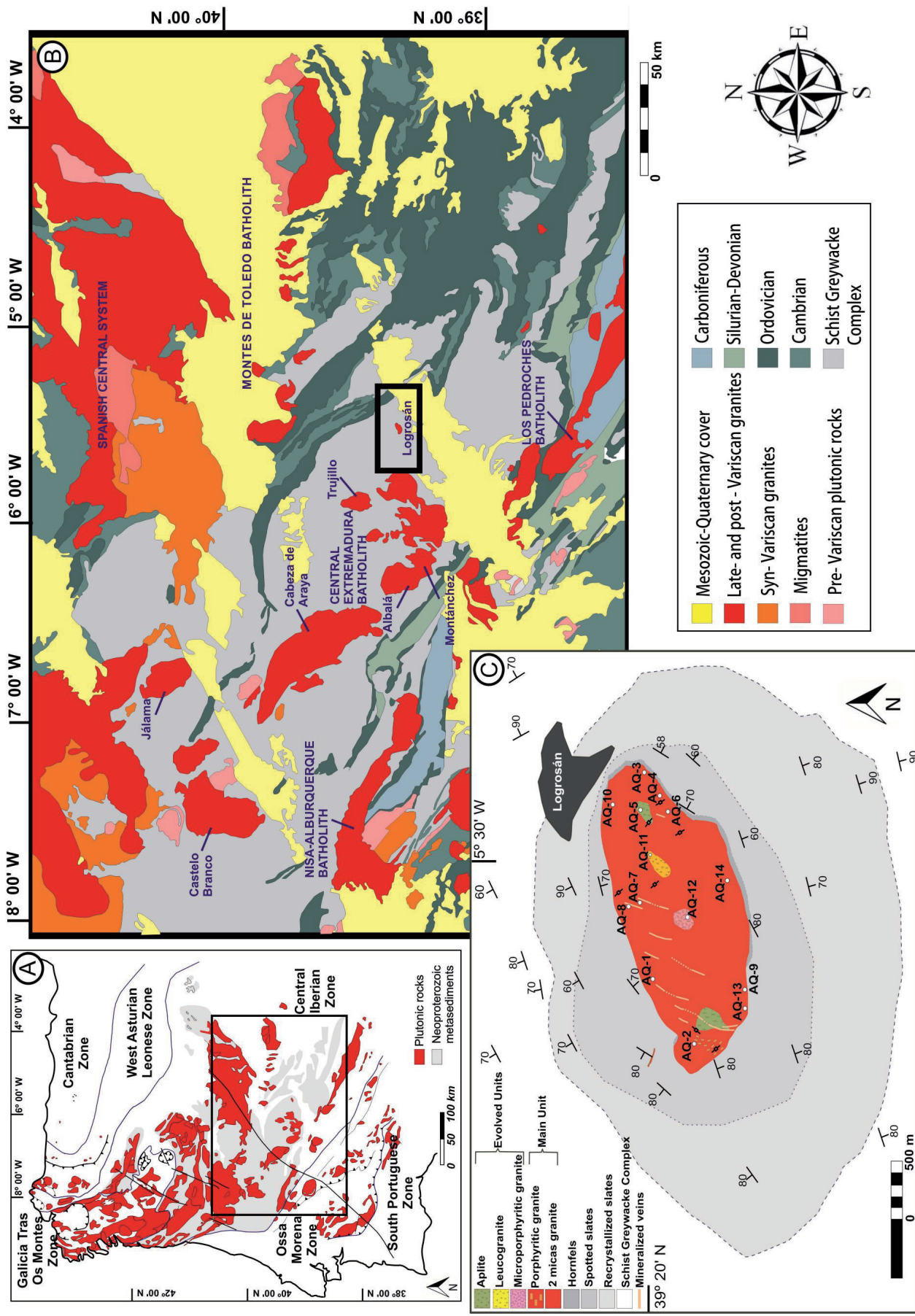


Fig. 1.- (a) Schematic geological map of the Logrosán granite and its location within the Iberian Massif. (b) Regional geological sketch displaying the studied area (modified from Rodriguez *et al.*, 2008). (c) Detail of the Logrosán granite. Sampling points are indicated by open circles

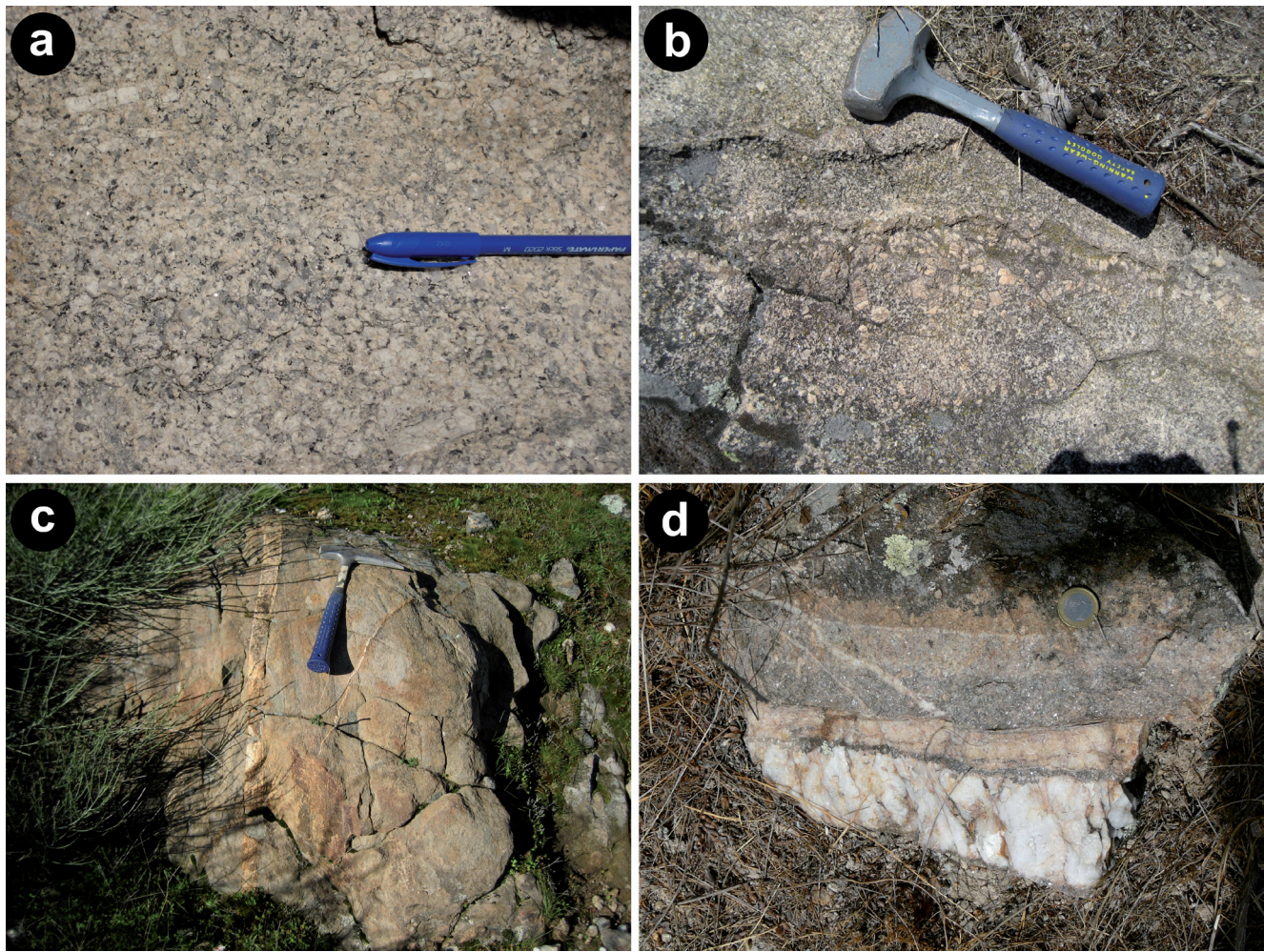


Fig. 2.- Field features of the Logrosán granite. (a) Two-mica granite with coarse to medium grain of the Main Unit. (b) Porphyritic sectors in the Main Unit granite. (c) Aplitic of the Evolved Units and barren quartz veins cutting through it. (d) Greisen vein selvage. Note the pervasive muscovitization of the original granitic rock.

### 3. Field relations and petrography

The Logrosán granite is an evolved leucogranitic apophysis with an outcropping area of about 4 km<sup>2</sup> (Fig. 1c). This body shows a sub-ellipsoidal shape elongated in the NE-SW direction, and a hidden larger volume of granite rocks may be assumed by the extent of the contact-metamorphic area. The Logrosán pluton is mainly composed of a coarse- to medium-grained two-mica leucogranite (Main Unit) (Fig. 2a) which grades to fine-grained or porphyritic varieties (Fig. 2b). Where K-feldspar megacrysts appear, flow textures are visible with a N130 main trend, following the contact of the granitic pluton in the most external areas. The two summits of the hill defined by the Logrosán granite (the San Cristóbal hill) are composed of a microporphyritic (two-texture) granite and an aplitic granite (Evolved Units) (Fig. 2c). No sharp contacts between the Evolved Units and the Main Unit could be observed. Pegmatitic and fine-grained leucocratic bodies of variable size are frequent and usually showing sharp contacts with the Main Unit. Micaceous, mostly biotitic enclaves are occasionally found, as well as schlieren structures. The

bulk of the stock is composed of quartz, plagioclase, K-feldspar, muscovite, biotite and accessory minerals (tourmaline, apatite, zircon, monazite, ilmenite, Nb-rich rutile).

Tourmaline appears as an accessory phase within most of the Logrosán granite units, even in some pegmatitic miaroles. Tourmaline is also associated with all types of quartz-veining systems that cross-cut the granite body and occurs within the granite-metasediment contact. The Logrosán granite was triggered by complex hydrothermal events which are identified by the presence of sectors with a dense network of quartz-rich veining (cm-scale in thickness of barren-, tourmaline-, cassiterite-rich varieties). Therefore, greisen-type alteration zones are found in the areas with a high proportion of mineralized veins and veinlets (Chicharro et al., 2011). Greisen alteration is not only restricted to the selvages but also affects some parts of the granitic body (Fig. 2d). This alteration is characterized by high contents of muscovite and the presence of disseminated cassiterite. A “sandy granite” is very common adjacent to the Sn-(W) veins and greisen alteration and in most cases is a result of old mining activity (processing/panning for mineral recovery).

#### 4. Analytical methods

A total of 9 representative samples weighted between 3-5 kg were collected for whole-rock geochemistry (6 medium to coarse-grained granites from the Main Unit and 3 fine-grained or microporphyritic granites from the Evolved Units) (Table 1). Fresh and less altered fractions of each sample were selected for crushing and powdering. Each sample was

fused using a lithium metaborate-tetraborate mixture. The melt produced by this process was completely dissolved with 5% HNO<sub>3</sub>. Major analyses were carried out using fusion-inductively coupled plasma mass spectrometer (FUS-ICPMS) while trace elements were analyzed by fusion-inductively mass spectrometer (FUS-MS) at Activation Laboratories (ACTLABS, Canada). Uncertainties in major elements are bracketed between 1 and 3% relative, except for MnO (5–

	Main granite				Evolved granites				
	AQ1 111911	AQ2 111912	AQ4 111976	AQ6 111978	AQ13 L178	AQ14 179	AQ5 111979	AQ11 L174	AQ12 L177
SiO <sub>2</sub>	72.46	72.26	72.53	73.93	73.12	74.03	72.94	72.73	74.01
Al <sub>2</sub> O <sub>3</sub>	14.43	14.76	15.24	15.14	14.92	14.94	15.30	14.42	14.83
FeO <sub>t</sub>	1.25	1.71	1.33	0.82	1.37	1.14	0.78	1.45	1.17
MnO	0.02	0.02	0.02	0.02	0.02	0.02	0.01	0.02	0.02
MgO	0.28	0.33	0.38	0.16	0.33	0.24	0.22	0.22	0.26
CaO	0.59	0.45	0.69	0.50	0.54	0.51	0.46	0.25	0.46
Na <sub>2</sub> O	3.68	2.67	3.31	3.87	3.31	3.42	3.27	2.95	2.95
K <sub>2</sub> O	4.46	4.75	4.88	4.19	4.42	4.53	4.83	4.35	4.63
TiO <sub>2</sub>	0.18	0.23	0.27	0.10	0.21	0.17	0.17	0.13	0.15
P <sub>2</sub> O <sub>5</sub>	0.50	0.47	0.57	0.57	0.49	0.46	0.54	0.51	0.55
LOI	1.33	2.55	1.62	1.51	1.47	1.08	1.95	1.98	1.74
Total	99.16	100.20	100.80	100.80	100.20	100.50	100.50	99.00	100.80
Sc	3.00	4.00	2.00	3.00	3.00	2.00	2.00	2.00	3.00
Be	15.00	23.00	16.00	11.00	14.00	18.00	7.00	19.00	9.00
V	7.00	12.00	10.00	< 5	13.00	10.00	< 5	10.00	9.00
Cr	< 20	< 20	< 20	< 20	< 20	< 20	< 20	280	180
Co	2.00	4.00	3.00	3.00	2.00	2.00	2.00	2.00	2.00
Ni	< 20	< 20	< 20	< 20	< 20	< 20	< 20	< 20	< 20
Cu	< 10	20.00	< 10	20.00	< 10	< 10	< 10	< 10	< 10
Zn	30.00	50.00	60.0	30.00	40.00	70.0	< 30	70.0	< 30
Ga	21.00	23.00	25.00	20.00	22.00	21.00	20.00	24.00	20.00
Ge	2.20	2.10	1.70	2.30	2.30	2.10	1.50	3.40	2.50
As	60.0	51.0	137	94.0	137	64.0	123	44.0	103
Rb	288	301	338	317	311	238	270	362	317
Sr	44.00	41.00	57.0	39.00	44.00	38.00	52.0	32.00	57.0
Y	6.90	5.20	7.60	5.50	7.60	9.60	5.40	3.30	6.60
Zr	76.0	80.0	118	43.0	82.0	77.0	74.0	60.0	62.0
Nb	8.70	11.70	10.10	13.60	11.40	9.00	9.60	15.90	11.10
Mo	< 2	< 2	< 2	< 2	< 2	< 2	< 2	< 2	< 2
Ag	< 0.5	0.50	< 0.5	< 0.5	< 0.5	0.70	< 0.5	< 0.5	< 0.5
In	< 0.1	0.10	< 0.1	< 0.1	< 0.1	< 0.1	< 0.1	0.10	< 0.1
Sn	50.0	67.0	33.0	35.0	49.0	11.00	37.00	29.00	53.0
Sb	0.50	0.40	< 0.2	0.70	< 0.2	0.30	0.90	< 0.2	0.50
Cs	59.5	88.0	74.4	50.2	54.6	26.7	70.3	51.6	145
Ba	224	241	290	138	226	178	219	152	225
La	13.80	16.10	21.80	6.53	15.10	13.00	11.40	8.81	9.67
Ce	31.40	35.60	50.20	14.80	33.10	27.70	27.80	19.20	20.70
Pr	3.58	3.85	6.42	1.74	3.95	3.34	3.25	2.17	2.48
Nd	13.30	14.50	25.80	6.40	15.60	12.90	12.50	8.06	10.00
Sm	2.96	3.05	5.18	1.56	3.25	2.94	2.92	1.73	2.47
Eu	0.32	0.32	0.47	0.21	0.33	0.30	0.32	0.19	0.36
Gd	2.24	2.21	3.35	1.44	2.54	2.52	2.22	1.26	2.24
Tb	0.33	0.29	0.46	0.25	0.36	0.40	0.35	0.18	0.35
Dy	1.52	1.35	1.85	1.20	1.64	1.87	1.50	0.84	1.75
Ho	0.24	0.21	0.26	0.19	0.25	0.32	0.22	0.12	0.24
Er	0.60	0.52	0.60	0.51	0.66	0.86	0.46	0.30	0.51
Tm	0.09	0.07	0.08	0.07	0.09	0.12	0.06	0.05	0.06
Yb	0.56	0.49	0.44	0.53	0.52	0.71	0.37	0.30	0.38
Lu	0.08	0.07	0.06	0.07	0.08	0.11	0.05	0.05	0.06
Hf	2.20	2.40	3.00	1.50	2.60	2.50	2.50	1.70	2.10
Ta	2.26	3.08	2.50	4.76	3.73	1.97	1.98	4.00	2.30
W	24.60	82.1	74.2	36.00	23.90	9.00	131	1.60	376
Tl	1.84	1.98	2.02	1.99	1.87	1.40	1.77	1.56	1.79
Pb	28.00	22.00	29.00	21.00	24.00	28.00	26.00	21.00	29.00
Bi	0.30	< 0.1	0.60	1.50	0.30	2.60	0.40	< 0.1	0.60
Th	7.59	8.28	19.90	3.07	8.70	6.65	8.67	5.30	4.45
U	7.91	7.25	10.90	8.49	7.04	11.00	10.50	9.04	7.23
F		2003	1611	1150			1053		
Li		290	303	141			209		
T (°C)*	738	755	777	699	752	746	744	734	733

\*Temperatures estimated using the saturation zircon temperature of Watson and Harrison (1983)

Table 1.- Whole-rock major (wt. %), trace-element and REE (ppm) compositions of the Logrosán granite

10%). The precision for Rb, Sr, Zr, Y, V, Hf and most of the REE range from 1 to 5%, and between 5 and 10% for the rest of trace elements. Some granite samples have concentrations in transition metals below detection limits (V: 5 ppm, Cr: 20 ppm, Sc: 1 ppm, Co: 10 ppm) and almost all the granites have Ni < 20 ppm and Mo < 2 ppm. More information on the procedure, precision and accuracy of ACTLABS ICP-MS analyses can be found at [www.actlabs.com](http://www.actlabs.com).

Fluorine and Lithium were determined in selected samples in the laboratory of the Spanish Geological and Mining Institute (IGME), where F was determined by spectrophotometric methods after its extraction by pyrohydrolysis and Li was extracted by digestion with HF-HNO<sub>3</sub>-HClO<sub>4</sub> and determined by atomic absorption spectrophotometry. An analytical error of ± 10% has been estimated.

Stable isotope data were obtained at the Stable Isotope Laboratories of the Salamanca University (Spain). Whole rock samples of unaltered granite were analyzed for oxygen and hydrogen isotope composition (Table 2). <sup>18</sup>O/<sup>16</sup>O determinations for whole rock samples were carried out by laser fluorination using a conventional vacuum extraction line employing ClF<sub>3</sub> as the reagent (Borthwick and Harmon, 1982; Clayton and Mayeda, 1963). H<sub>2</sub> and H<sub>2</sub>O extraction for D/H isotopic analysis for whole rock samples were carried out by the uranium technique described by Godfrey (1962) with modifications introduced by Jenkin (1988) heating the samples at temperatures up to 1500 °C. Oxygen and hydrogen isotope ratios were measured in a SIRA-II mass spectrometer and data are reported in the normal denotation relative to V-SMOW.

Sr-Nd isotopic compositions were measured on six representative granites (Table 2) at the Centro de Asistencia a la Investigación (CAI) of Geochronology and Isotope Geochemistry (Complutense University of Madrid, Spain). Whole-rock samples were dissolved in ultra-pure reagents and the isotopes were subsequently isolated by exchange chromatography. Isotope analyses were carried out using a Sector 54 VG Multicollector Thermal Ionization Mass Spectrometer with data acquired in multidynamic mode. Repeated analyses on the NBS-987 standard gave <sup>87</sup>Sr/<sup>86</sup>Sr = 0.710240 ± 0.00005 (2σ, n = 8) and for the La Jolla standard, values

of <sup>143</sup>Nd/<sup>144</sup>Nd = 0.511847 ± 0.000003 (2σ, n = 14) were obtained.

Individual zircon and monazite crystals were separated for geochronology and Lu-Hf isotopic studies from a mixture of two representative granite samples (AQ1 and AQ2, see Table 1). About 5 kg granite of each sample were crushed and sieved with a steel jaw-crusher and a disk mill at the Complutense University of Madrid. Zircon and monazite were preconcentrated with a Wifley table using a modified version of the “water-based” separation technique of Söderlund and Johansson (2002) at the Spanish Geological Survey laboratories (IGME, Tres Cantos, Spain). Further separation based on paramagnetic properties was done using a Franz isodynamic separator. Finally the zircon and monazite selected for analyses were hand-picked under a microscope. Several monazite and zircon crystals were carefully selected by picking the most idiomorphic crystals to avoid all possibility of inheritance for ID-TIMS. A representative selection of zircons were strewn and mounted on epoxy resin for LA-ICPMS microanalysis. The mount was polished to expose the zircon central portions and studied with transmitted and reflected light on a petrographic microscope. The internal structure, inclusions, fractures and physical defects were analyzed using back scattered electron (BSE) imaging.

The zircon fractions selected for ID-TIMS were pre-treated with the chemical abrasion (CA) method of Mattinson (2005). Zircon annealing was carried at 900°C for 48 hours and the chemical attack was done in Parrish-type minibombs inside Parr bombs at 180°C for 12 hours. Final zircon dissolution was achieved after placing the bomb at 240°C for 72 hours. The procedure for extraction and purification of Pb and U is a scale-down version of that of Krogh (1973). A <sup>208</sup>Pb-<sup>235</sup>U spike was used to obtain the U/Pb ratios by isotope dilution (ID). Isotopic ratios were measured with a Triton TIMS multi-collector mass spectrometer equipped with an axial secondary electron multiplier (SEM) ion counter. The instrument is set up to do measurements both in static and peak-jumping mode using the SEM. For static measurements the <sup>204</sup>Pb was measured with the calibrated SEM (92-93% Yield calibration). The Pb measurements were done in the 1300-1460°C range, and U was measured in the 1420-1500°C

Sample	Rock type	Age (Ma)	Rb	Sr	<sup>87</sup> Rb/ <sup>86</sup> Sr	<sup>87</sup> Sr/ <sup>86</sup> Sr	±2σ	( <sup>87</sup> Sr/ <sup>86</sup> Sr) <sub>t</sub>	Sm (ppm)	Nd (ppm)	<sup>147</sup> Sm/ <sup>144</sup> Nd	<sup>143</sup> Nd/ <sup>144</sup> Nd	±2σ	( <sup>143</sup> Nd/ <sup>144</sup> Nd) <sub>t</sub>	ε <sub>Nd</sub> <sup>t</sup>	TDM	δ <sup>18</sup> O <sub>SMOW</sub>	δD <sub>SMOW</sub>	H <sub>2</sub> O %
AQ2	main granite	308	301	41	21.487	0.822394	4	0.728213	3.05	14.50	0.1272	0.512294	2	0.512037	-4.0	1.32	14.1	-84.7	1.4
AQ6	main granite	308	317	39	23.806	0.829387	6	0.725042	1.56	6.40	0.1474	0.512321	2	0.512024	-4.2	1.62			
AQ13	main granite	308	311	44	20.657	0.807511	3	0.716966	3.25	15.60	0.1259	0.512290	1	0.512036	-4.0	1.31			
AQ3	altered granite	308	411	28	43.362	0.918694	6	0.728633	2.76	11.10	0.1503	0.512325	1	0.512022	-4.3	1.67			
AQ10	altered granite	308	361	77	13.658	0.774096	4	0.714232	4.90	19.50	0.1519	0.512343	1	0.512036	-4.0	1.67			
AQ5	evolved granite															14.5	-77.9	1.3	
AQ12	evolved granite	308	317	57	16.216	0.783536	3	0.712459	2.47	10.00	0.1493	0.512327	2	0.512026	-4.2	1.65	15.0	-77.0	1.2

Table 2.- Sr-Nd and O-D isotopic data of the Logrosán granite

interval (for further analytical details see Rubio-Ordóñez *et al.*, 2012). Data reduction was done using the PbMacDat spreadsheet (Isachsen *et al.*, 2007; [www.earth-time.org](http://www.earth-time.org)). All isotopic ratios are corrected for mass fractionation, blank and initial common Pb after the model of Stacey and Kramers (1975). Ages and uncertainties were calculated with the decay constants of Jaffey *et al.* (1971), and are reported at the  $2\sigma$  level. The concordia age was calculated and the data were plotted with Isoplot 3.0 (Ludwig, 2003).

$\text{U-Pb}$  *in situ* age determinations were carried out on 37 polished zircons using a New Wave Research LUV213 laser-ablation microprobe, attached to an Agilent 7500 quadrupole ICP-MS at the ARC GEMOC Centre of the Macquarie University, Sydney (Australia). A laser beam of 30  $\mu\text{m}$  diameter with energies of 60-100 mJ/pulse and 5 Hz repetition rate was shot during 100-120 s resulting in pits of about 30  $\mu\text{m}$  deep. Real-time data were processed using the GLITTER® software package. The correction factors were then checked using the GEMOC-GJ-1 with a TIMS age of 608.5 Ma, the Mud Tank zircon ( $734 \pm 32$  Ma, Black and Gulson, 1978) and the 91500 international zircon standard (1064 Ma, Wiedenbeck *et al.*, 1995). Concordia diagrams ( $2\sigma$  error ellipses), concordia ages and upper intercept ages were calculated using the Isoplot/Ex software (Ludwig, 2003).

*In situ* Hf isotopic measurements were performed on 28 previously dated zircon spots at the ARC GEMOC Centre of the Macquarie University. Analyses were carried out using a New Wave Research LUV213 laser-ablation microprobe, attached to a Nu Plasma multi-collector (MC) inductively coupled plasma mass spectrometer (ICPMS). The laser system delivers a beam of 213 nm UV light from a frequency-quintupled Nd:YAG laser. The laser was fired with energy of 5-7 J/cm<sup>2</sup>, laser beam diameter was 30  $\mu\text{m}$  and repetition rate was 5 Hz. The laser beam ablated the zircon surface during 100-120 s resulting in pits 30  $\mu\text{m}$  deep. The analytical methods are the same as described in detail by Griffin *et al.* (2002; 2004). To evaluate the accuracy and precision of the laser ablation results we have repeatedly analyzed two zircon standards: 91500 and Mud Tank (MT). These reference zircons gave  $^{176}\text{Hf}/^{177}\text{Hf} = 0.282310 \pm 0.000049$  ( $2\sigma$ ) and  $0.282502 \pm 0.000044$  ( $2\sigma$ ), respectively, which are identical to average published values of  $0.282306 \pm 0.000008$  for 91500 and  $0.282507 \pm 0.000006$  for MT (Woodhead and Herdt, 2005). The  $2\sigma$  uncertainty on a single analysis of  $^{176}\text{Lu}/^{177}\text{Hf}$  is  $\pm 0.001$ - $0.002\%$  (about 1 epsilon unit), reflecting both analytical uncertainties and the spatial variation of Lu/Hf across many zircons. The  $^{176}\text{Lu}$  decay constant value of  $1.865 \times 10^{-11}\text{a}^{-1}$  was used in all calculations (Scherer *et al.*, 2001). Chondritic  $^{176}\text{Hf}/^{177}\text{Hf} = 0.282772$  and  $^{176}\text{Lu}/^{177}\text{Hf} = 0.0332$  (Bouvier *et al.*, 2008) and the depleted mantle  $^{176}\text{Hf}/^{177}\text{Hf} = 0.28325$  ( $\epsilon\text{Hf} = +16.4$ ) and  $^{176}\text{Lu}/^{177}\text{Hf} = 0.0384$  were applied to calculate  $\epsilon\text{Hf}$  values and model ages used in this work.

The trace element zircon composition was obtained by laser ablation (LA-ICPMS) at the Natural History Museum of London (NHM, London, UK) using an Agilent 7500CS ICP-

MS coupled to a New Wave UP213 laser source (213 nm frequency-quadrupled Nd-YAG laser). The diameter of the laser beam was 10  $\mu\text{m}$ . A 40 s gas blank was analyzed first to establish the background, followed by 50 s measurements for the remainder of the analysis. Each analysis was normalized to Si using concentrations determined by electron microprobe. Relative element sensitivities were calibrated with a NIST 612 glass standard.

## 5. Results

### 5.1. Whole-rock geochemistry

The results of major, minor and trace element analyses of nine granite samples are presented in Table 1. The Logrosán granite shows high  $\text{SiO}_2$  (63.59-74.03 wt.%),  $\text{P}_2\text{O}_5$  (0.42-0.78 wt.%) and  $\text{Al}_2\text{O}_3$  (14.42-15.38 wt.%), but very low  $\text{CaO}$  (0.25-0.69 wt.%) contents (Table 1). The Logrosán granite has a strong peraluminous character, with an alumina-saturation index ranging from 1.22 to 2 and high normative corundum contents (3.55-8.42%).

In variation diagrams using  $\text{TiO}_2$ , Logrosán samples do not define clear fractional crystallization trends, except for the  $\text{MgO}$ , which markedly decreases towards the more evolved samples (Fig. 3). Although there is some scatter in the, generally the  $\text{Al}_2\text{O}_3$ ,  $\text{FeO}$ ,  $\text{MgO}$ ,  $\text{CaO}$  and  $\text{K}_2\text{O}$  contents decrease while the  $\text{SiO}_2$ ,  $\text{Na}_2\text{O}$  and  $\text{P}_2\text{O}_5$  contents increase. Scatter is mainly found in a slightly leached albited sample which behaves discordantly to other samples of the Main Unit (e.g. AQ6, see Table 1 and Figs 3 and 4). However, more evolved granites (Evolved Units) seem to form discrete trends for certain major elements such as  $\text{CaO}$  and  $\text{K}_2\text{O}$ . Their depletion would be consistent with plagioclase and alkali feldspar fractionation, but they show different evolution trends for the Main and Evolved Units.

Granite REE patterns show a variable fractionation ( $\text{La}_{\text{N}}/\text{Yb}_{\text{N}} = 8.37$ - $33.6$ ) but are generally highly fractionated, with a negative Eu anomaly for granites of the Main Unit ( $\text{Eu}/\text{Eu}^* = 0.32$ - $0.42$ ) and slightly more negative towards granites of the Evolved Units ( $\text{Eu}/\text{Eu}^* = 0.37$ - $0.45$ ) (Fig. 4). In trace-element chondrite normalized diagrams, the Logrosán samples show negative anomalies in Ba, Nb, Sr and Ti (Fig. 4). The negative Eu anomaly and the low Sr contents of the granite suggest that plagioclase fractionation has occurred for both Main Unit and Evolved Units. In variation diagrams Ba, Rb, Sr, Eu, Cs, Y, Th, HREE and LREE become depleted with increasing degree of fractionation (Fig. 3). As with major elements, Evolved granite Units show different trends for some elements (e.g., Rb, Fig. 3) compared to the Main Unit set of samples.

The HFSE show no clear trend with granite differentiation. A slight tendency of increasing Nb and Ta can be recognized, while Sn exhibits a wider scatter (Fig. 3). High Sn contents found in this granite with respect to the crustal average (i.e. granites with Sn contents higher than 10 ppm, as defined by

Flinter, 1971) allow classifying it as stanniferous granite. Ga and Hf data display trends where more fractionated samples show the lowest contents. The overall range for Ga and Hf concentration is quite restricted (Ga: 20-25 ppm and Hf: 1.5-3.0).

### 5.2. Oxygen isotopes

Whole rock and quartz  $\delta^{18}\text{O}$  results on Logrosán samples gave a narrow range between 14.1 and 15.0‰ (vs. SMOW) showing a positive correlation with  $\text{SiO}_2$  of the rock (Table 2).  $\delta^{18}\text{O}$  values higher than 10‰ have been observed in many Variscan granites from western Europe (Tartèse and Bouvais, 2010; Hoefs and Emmermann, 1983) and are typical for high- $\text{SiO}_2$  peraluminous granites (Taylor, 1978). Similar  $\delta^{18}\text{O}$  values have been found in other granites from the southern CIZ (e.g., Castelo Branco Batholith: 12.2-13.7‰, Antunes *et al.*, 2008). Nevertheless, these values are significantly higher than those found in the peraluminous S-type granites of the Spanish Central System, which mostly range from 8.3 to 10.2‰ (Villaseca and Herreros, 2000; Recio *et al.*, 1992).

### 5.3. Sr-Nd isotopes

The measured Sr and Nd isotope ratios were recalculated back to 300 Ma based on the intrusion age determined in the section 5.5 (U-Pb geochronology). The Logrosán granite is characterized by a large variation in initial  $^{87}\text{Sr}/^{86}\text{Sr}$  ratios (from 0.7125 to 0.7286) whereas  $\epsilon\text{Nd}$  is much less variable (between -4.3 and -4.0) (Table 2). The Sm-Nd model ages were calculated using the equation of Liew and Hofmann (1988) (Table 2) (Fig. 5). The obtained model ages (1.31-1.67 Ga) are similar to those given for other peraluminous monzogranites and leucogranites from the Central Extremadura Batholith (e.g., Antunes *et al.*, 2008; Castro *et al.*, 1999).

### 5.4. Zircon description and composition

A total of 68 zircon grains were selected. 37 grains were dated by U-Pb and 28 were analyzed for their Hf-isotope composition. Based on the morphology, we have distinguished two groups of zircon grains: (1) euhedral elongated bipyramidal prisms and (2) stubby prisms. Most of the ana-

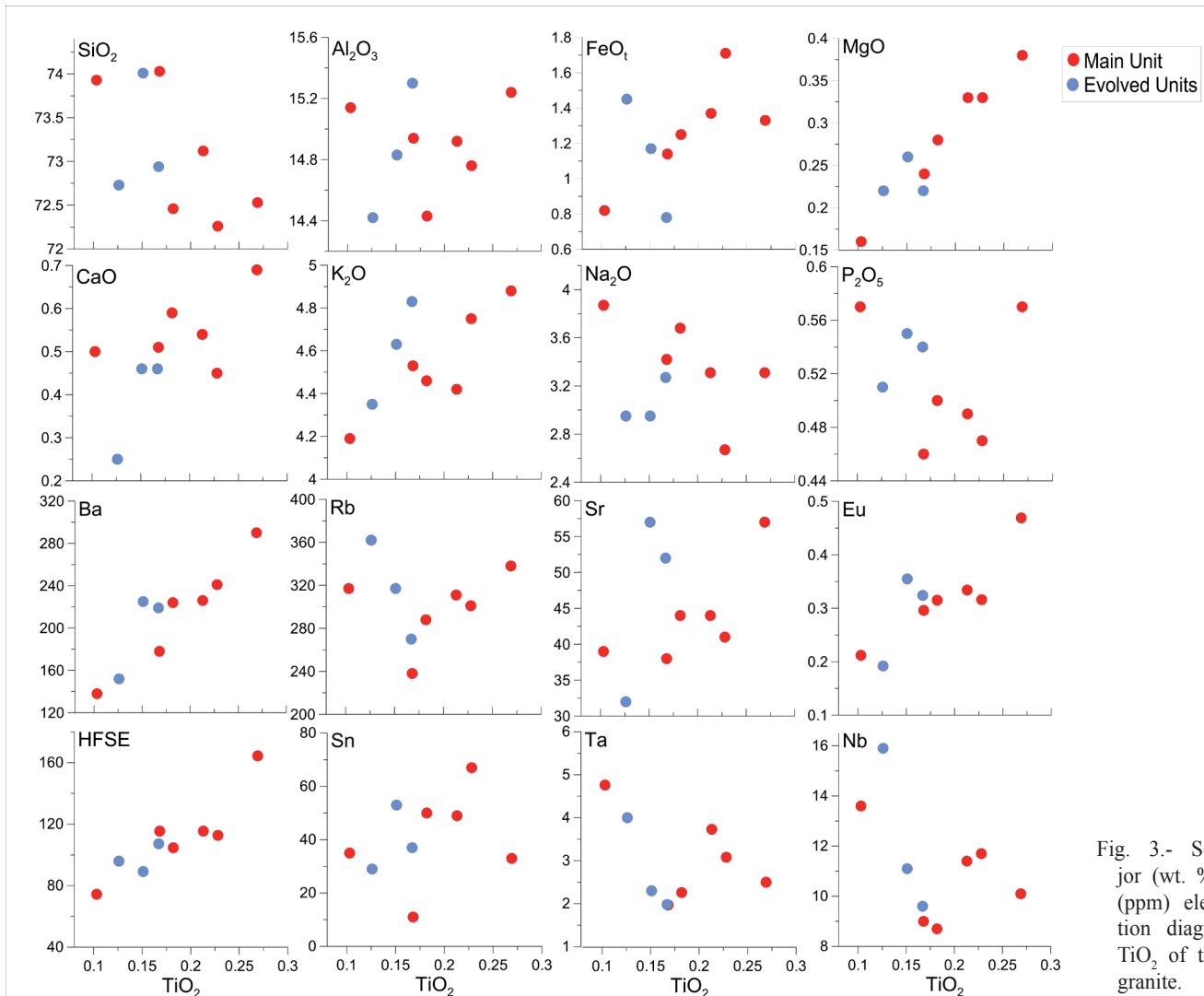


Fig. 3.- Selected major (wt. %) and trace (ppm) element variation diagrams versus  $\text{TiO}_2$  of the Logrosán granite.

lyzed grains (about 67%) belong to the first group. This population is characterized by sizes ranging from 100 to 200  $\mu\text{m}$  and aspect ratios ranging from 1:6 to 1:2, being dominantly 1:2 (Fig. 6, e.g., L24-20 and L30-31). The second zircon type comprises stubby prisms (1:1 aspect ratio) of usually smaller grain size (average size of 100  $\mu\text{m}$ ) (Fig. 6, e.g., L24-12). The BSE images show that most zircon grains have homogeneous or sector-zoned inner cores with dark thin rims (Fig. 6, e.g. L24-01). Stubby zircons sometimes present texturally discordant dark cores and/or fine euhedral oscillatory zoning (Fig. 6, L30-22).

Logrosán zircons show negative Eu anomalies ( $\text{Eu}^*/\text{Eu} < 0.3$ ) and relatively high REE (647-2435 ppm), Nb (1.17-5.24 ppm), Ta (0.31-3.92 ppm), Sc (157-939 ppm) and Hf (7631-11800 ppm) contents, characteristic of zircon from granitoid rocks (Hoskin and Schaltegger, 2003; Belousova *et al.*, 2002) (Table 3). Zircon REE abundances normalized to chondrite values (McDonough and Sun, 1995) show steeply-rising slopes from the LREE to the HREE. Euhedral elongated bipyramidal prismatic crystals (type-1) are generally Variscan-age zircons and usually richer in Hf than inherited zircons, which are mainly stubby (type-2) (Fig. 6). This is in accordance with the fact that the abundance of Hf in igneous zircons is considered as a marker of the degree of magma differentiation (Hoskin and Schaltegger, 2003). Hf correlates positively with P, Y, Th, U, Nb, Ta, HREE and LREE, whilst it shows a negative correlation with Zr/Hf (Fig. 7). The positive correlation of P, Y and HREE with Hf reveals that “xenotime” substitution mechanism is the dominant substitution in the Logrosán zircon (Speer, 1982). Experiments on Zr/Hf fractionation in zircon-crystallizing melts unravel a decrease of the Zr/Hf ratio of the residual melt related to an increase of the abundance of  $\text{HfO}_2$  in zircon for fractional crystallization of peraluminous granitic melts (Linnen and Keppler, 2002). Then, the decrease in Zr/Hf with increasing Hf observed in the Logrosán zircon can be explained by crystal fractionation. Likewise, the behavior of incompatible elements, such as Th, U, Nb and Ta, which increase correlatively with Hf in zircon, denotes an enrichment of these elements in the melt as the magma evolves.

### 5.5. U-Pb geochronology

Seven zircon fractions and one monazite fraction were analyzed by ID-TIMS. All zircon fractions were pre-treated to remove Pb loss, before final dissolution, with the chemical abrasion (CA) method of Mattison (2005). Only one zircon fraction (Z7), a single grain, plots in a discordant position which could be attributed to partial secondary Pb-loss (see Krogh, 1982). The remaining data are either concordant or scattered due to the presence of older xenocrystic zircon.

Five fractions (zircon fractions Z3, Z5, Z8, Z6 and monazite fraction M1) are concordant and plot between 307 and 310 Ma. The remaining zircon fractions (Z1, Z2 and Z4) are discordant due to the presence of inherited zircons. These are

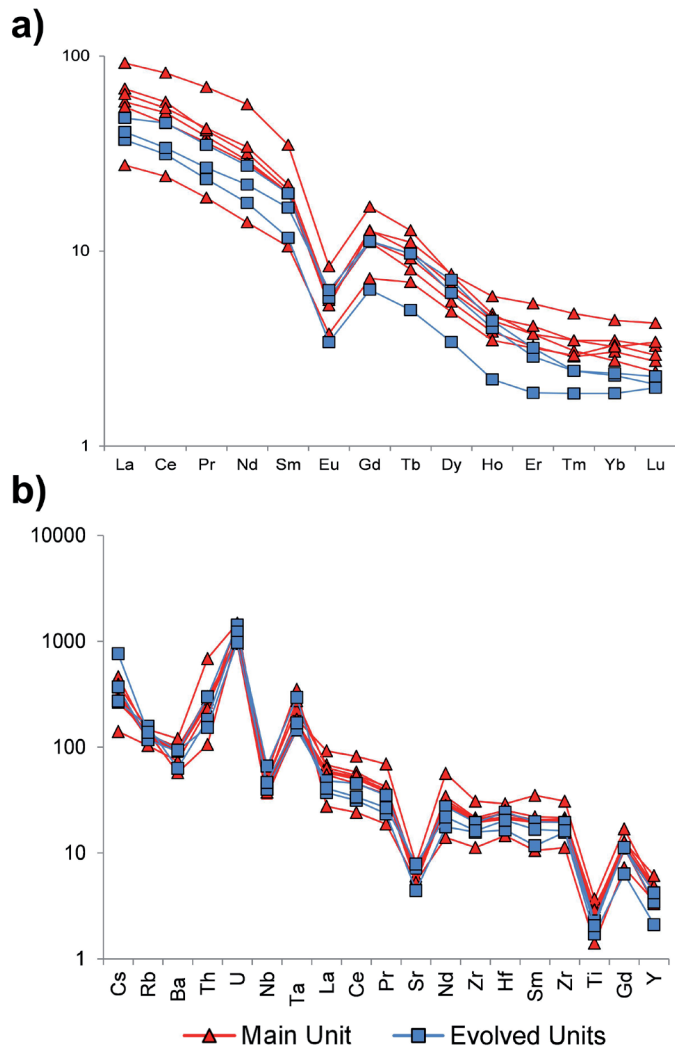


Fig. 4.- Chondrite-normalized REE diagram (a) and Chondrite-normalized multi-trace element diagram (b) of the Logrosán granite.

multigrain (made up of 25 crystals) to some single crystal fractions (Table 4). The concordant fractions Z3 and Z5 and the discordant fractions Z2 and Z4 define a mixing line (Line 1; Fig 8a) which has an upper intercept of ca. 1.1 Ga suggesting a Mesoproterozoic inheritance. The concordant fractions Z3 and Z5 and the discordant fraction Z1 also define a mixing line (Line 2; Fig 8a) which has an upper intercept of ca. 550-560 Ma pointing to an additional Late Neoproterozoic inherited component. These are very long projections, so the validity of the age of the inherited component has been constrained by *in-situ* U-Pb ages (see LA-ICPMS data below).

The age of the intrusion of the Logrosán granite is constrained by the cluster of analyses on the Concordia curve between 307 and 310 Ma (fractions Z3, Z5, Z8, Z6 and M1; Table 4). Fraction Z6, a single zircon, is slightly older suggesting the possible presence of an inherited component. Zircon fractions Z3, Z8 and Z5 and the monazite fraction M1 overlap at 307-308 Ma (Fig 8a). These four fractions provide a combined “Concordia” age of  $307.88 \pm 0.86$  Ma with an MSWD of 1.8 (decay constant errors included). This age

Sample	L30-27	L24-17	L24-1	L24-20	L30-30	L24-19	L24-16	L24-6	L24-20	L30-31	L24-10	L24-9	L30-28	L24-12
Age*	V	V	V	V	V	V	V	V	V	V	V	O-I	PO-I	PO-I
P	409	274	516	409	430	674	328	1233	692	613	585	322	430	942
Sc	244	392	222	556	381	157	323	939	564	625	627	157	253	580
Ti	19.78	18.40	22.84	7.37	12.65	11.21	21.04	5.89	19.14	61.60	12.34	56.71	22.96	15.70
Y	1780	1960	1560	3630	2280	1440	1240	3612	1622	1082	934	1060	1840	917
Nb	1.67	2.70	1.57	5.24	4.64	1.66	1.62	4.11	1.77	1.86	1.75	1.61	1.17	4.21
Ta	0.52	0.88	0.50	1.60	1.53	0.55	0.44	1.34	0.57	0.49	0.46	0.41	0.31	3.92
Hf	8490	10100	8680	9740	11800	9150	8970	11524	9565	10633	7631	8370	9800	8471
Pb	6.54	8.47	4.53	6.37	39.50	21.50	5.94	5.30	5.64	8.32	5.08	4.07	5.30	15.72
Th	179	234	159	236	852	750	202	149	185	236	148	127	182	353
U	601	1050	384	577	1530	763	511	772	395	403	568	179	243	740
La	0.24	1.07	0.11	<0.06	2.21	<0.06	<0.06	0.513	0.224	0.25	0.39	0.303	<0.06	2.37
Ce	4.41	9.28	4.53	5.18	33.6	7.12	3.06	5.18	4.79	3.70	4.21	3.46	2.61	19.9
Pr	0.51	1.44	0.65	0.22	8.37	0.59	0.32	0.39	0.77	0.60	0.68	0.43	0.49	4.68
Nd	7.22	11.7	9.79	3.81	68.1	9.26	5.74	4.36	11.1	7.6	7.24	6.26	8.27	33.4
Sm	14.7	16.0	15.6	12.0	46.3	15.1	11.3	9.83	15.6	11.8	8.92	9.21	15.8	21.8
Eu	0.45	1.07	0.74	0.83	2.03	0.43	0.39	0.62	0.77	0.34	0.40	0.55	0.55	1.19
Gd	58.20	59.10	57.10	82.60	99.60	55.80	40.00	61.93	59.12	41.23	33.21	35.30	65.50	44.28
Tb	18.60	19.80	17.30	29.90	27.50	15.80	12.20	23.48	16.34	11.17	9.32	10.40	18.80	11.66
Dy	206	209	179	366	262	163	128	312	180	117	98.2	114	197	108
Ho	65.8	68.1	54.6	127	78.8	53.2	42.7	113.6	55.65	37.58	31.61	37.6	65.3	30.9
Er	260	284	229	549	319	218	186	505	222	156	130	161	277	119
Tm	55.10	58.30	45.00	110.0	66.20	44.60	40.50	104.2	43.72	31.43	26.91	33.10	54.60	25.31
Yb	531	568	413	1000	626	412	406	935	390	286	254	315	485	236
Lu	72.00	82.00	58.30	148.0	100.0	58.50	60.90	160.7	60.49	49.18	41.88	50.50	79.60	36.53
LREE	85.72	99.66	88.53	104.6	260.2	88.30	60.82	82.82	92.37	65.56	55.05	55.52	93.22	127.6
HREE	1209	1289	996	2330	1480	965	876	2154	968	688	592	722	1177	567
Zr/Hf	50.19	47.32	51.11	47.39	40.53	49.98	49.35	42.74	47.86	45.18	55.40	55.16	49.06	44.01
T (°C)**	872	863	889	766	821	808	879	744	868	1024	818	1012	890	845

\* V Variscan-age zircon, PO-I pre-Ordovician inheritance, O-I Ordovician inheritance.

\*\* Temperatures estimated using the Ti-in-zircon geothermometer recalibrated by Ferry and Watson (2007). Temperatures uncertainty for each data is ±4.5%

Table 3.- LA-ICPMS trace element composition and REE (ppm) of zircons from the Logrosán granite

Sample	Weight (mg)	Concentration			Isotopic ratios						Apparent ages (Ma)				
		U (ppm)	Pb (ppm)	Common Pb (pg)	$^{206}\text{Pb}^*/^{204}\text{Pb}$	$^{206}\text{Pb}/^{238}\text{U}$	% (2s)	$^{207}\text{Pb}/^{235}\text{U}$	% (2s)	$^{207}\text{Pb}/^{206}\text{Pb}$	% (2s)	Rho	$^{206}\text{Pb}/^{238}\text{U}$	$^{207}\text{Pb}/^{235}\text{U}$	$^{207}\text{Pb}/^{206}\text{Pb}$
Z4 (A9)20smpr	120	101	8.0	231	134	0.05183	0.46	0.3895	0.91	0.05451	0.76	0.56	325.7	334.0	392.0
Z1(A5)25smpr	100	81	4.4	33	583	0.05005	0.25	0.3651	0.44	0.05291	0.35	0.60	314.8	316.0	324.7
Z2(A7)11medpr	80	125	6.6	38	617	0.04952	0.31	0.3602	0.80	0.05276	0.73	0.40	311.6	312.4	318.4
Z3 (A8)3larpr	60	111	8.5	93	154	0.04889	0.44	0.3540	1.04	0.05251	0.90	0.52	307.7	307.7	307.5
Z5(L1)3xtls	30	57	2.9	4	1063	0.04882	0.19	0.3540	0.75	0.05250	0.69	0.44	307.3	307.3	307.2
Z6(L4)Single	30	61	3.2	6	724	0.04936	0.43	0.3586	0.56	0.05269	0.35	0.78	310.6	311.1	315.3
Z7(L2)2xtls+1fra	60	63	3.0	4	1542	0.04771	0.43	0.3465	0.60	0.05266	0.41	0.73	300.5	302.0	314.3
Z8(L3)Single	30	92	4.6	7	918	0.04907	0.42	0.3557	0.50	0.05257	0.27	0.85	308.8	309.0	310.1
M1(X7)2xtls	20	5849	548	412	784	0.04883	0.24	0.3540	0.25	0.05258	0.08	0.95	307.3	307.7	310.9

Z, zircon, number of crystals; sm., small (ca. 80µm); med., medium (100-120µm); lar., large (120-180µm); pr., euhedral prisms (1:5 width/length ratio); el., elongated (1:7 width/length ratio); s.xtl., single crystal (>180µm). All zircon fractions were chemically abraded (CA technique after Mattinson (2005)). M, monazite. \* Ratio corrected for mass fractionation ( $0.11 \pm 0.02\%$  AMU Pb;  $0.10 \pm 0.02\%$  AMU U), spike contribution and analytical blank (6 pg Pb; 0.1 pg U). The other isotopic ratios are also corrected for initial common Pb after the model of Stacey and Kramers (1975). Rho, error OREJ correlation coefficient of the  $^{207}\text{Pb}/^{235}\text{U}$  and  $^{206}\text{Pb}/^{238}\text{U}$  ratios. Data reduced with PbMacDat (Isachsen et al. 2007; www.earth-time.org)

Table 4.- U-Pb ID-TIMS data of zircon and monazite fractions from the Logrosán granite

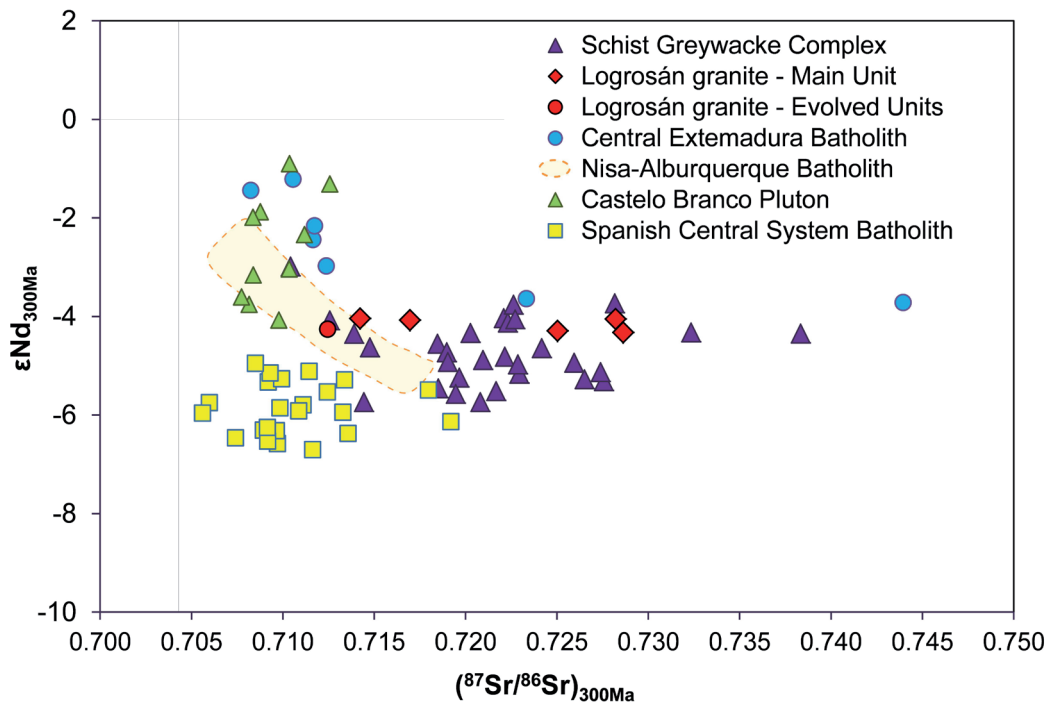


Fig. 5.- Initial Sr-Nd composition of the Logrosán granite and representative samples of other granites from the Central Extremadura Batholith (Castro *et al.*, 1999; Antunes *et al.*, 2008; González-Menéndez and Bea, 2004), the Spanish Central System (Villaseca *et al.*, 1998) and crustal protoliths of the Central Iberian Zone (Beetsma, 1995; López-Guijarro *et al.*, 2008; Ugidos *et al.*, 1997; Villaseca *et al.*, 2014). All data have been recalculated to a reference age of 300 Ma.

is considered the age of zircon and monazite crystallization, and therefore our most accurate estimate for the age of the granite intrusion.

The LA-ICPMS data set is listed in Table 4 and plotted in a concordia diagram (Fig. 8b). Ages younger than 1,000 Ma are 204-corrected  $^{206}\text{Pb}/^{238}\text{U}$ , whereas older ages are 204-corrected  $^{207}\text{Pb}/^{206}\text{Pb}$ . Thirty seven analyses were performed, 32 of which yielded concordant ages ranging from 294 to 1975 Ma. Five analyses were rejected due to high common-Pb or degree of discordance. Nineteen analyses yielded Variscan ages and 13 analyses yielded older-than-Variscan ages. A total set of 19 Variscan zircons provide a weighted average  $^{206}\text{Pb}/^{238}\text{U}$  age of  $303.0 \pm 2.3$  Ma (Fig. 8b). This weighted mean age is similar to that calculated using ID-TIMS data ( $307.88 \pm 0.86$  Ma) within uncertainty. We consider the ID-TIMS age of  $307.88 \pm 0.86$  Ma as the most accurate estimate for the age of the intrusion.

The thirteen older-than-Variscan ages represent 40% of inheritances. These ages are mostly Upper Neoproterozoic (from 550 to 847 Ma) ( $n = 8$ ) and have been obtained on dark anhedral to subhedral cores of stubby zircon (type-2) crystals; one of them was measured in a homogeneous dark core overgrown by a Variscan-age rim (L24-4, Table 5). Two youngest inherited zircon crystals show Cambrian (518 Ma) and Ordovician (447 Ma) ages (spots L24-18 and L30-30, Table 5) and are homogeneous stubby crystals. One Meso-proterozoic age of 1068 Ma was obtained on a homogenous dark core of a stubby zircon crystal (spot L30-28, Table 5 and Fig 6). The two oldest inherited zircons are Paleoproterozoic, 1950 and 1975 Ma (spot L24-5 and L20-35, respectively; Table 5), and correspond to stubby zircon crystals.

### 5.6. Hf isotope zircon composition

The zircon Lu-Hf isotopic data collected during this study are summarized in Table 6 and plotted as a function of their crystallization ages in figure 9. This figure also includes published data for zircon from the Spanish Central System Batholith (Villaseca *et al.*, 2012) and the Schist Greywacke Complex (Teixeira *et al.*, 2011). Depleted-mantle model ages ( $T_{\text{DM}}$ ) are useful to estimate the crustal residence age for the granite protolith (Andersen *et al.*, 2002).  $T_{\text{DM}}$  were calculated using the measured  $^{176}\text{Lu}/^{177}\text{Hf}$  ratios, referred to a model depleted mantle with a present-day  $^{176}\text{Hf}/^{177}\text{Hf} = 0.28325$  and  $^{176}\text{Lu}/^{177}\text{Hf} = 0.0384$  (Griffin *et al.*, 2000; 2002). These  $T_{\text{DM}}$  ages represent only a minimum age for the source of the host magma. Thus, a more realistic two-stage model ( $T_{\text{DM2}}$ ) has been used to estimate model ages of the source of the Logrosán granite.  $T_{\text{DM2}}$  were calculated assuming a  $^{176}\text{Lu}/^{177}\text{Hf}$  ratio of 0.015 for the average continental crust (Griffin *et al.*, 2000).

The Variscan zircon population yields initial  $^{176}\text{Hf}/^{177}\text{Hf}$  ratios of 0.282299-0.282758 which correspond to  $\epsilon\text{Hf}_{(t)}$  varying from +5.7 to -10.5, a range well outside of analytical uncertainties. The  $T_{\text{DM2}}$  range for Variscan zircon is accordingly wide and ranges from 928 to 1957 Ma but mostly between 1179 and 1594 Ma with a mean value of 1368 Ma which encompasses the values given by the whole rock Nd depleted model age (1.31-1.67 Ga). Neoproterozoic inherited zircons show initial  $^{176}\text{Hf}/^{177}\text{Hf}$  ratios of 0.281549 to 0.282735 which corresponds to  $\epsilon\text{Hf}(t)$  of +14.7 to -29.7, with more frequent  $\epsilon\text{Hf}(t)$  between +6.0 and -3.2. Meso to Paleoproterozoic zircons have  $^{176}\text{Hf}/^{177}\text{Hf}$  initial ratios of 0.281326-0.282007 and  $\epsilon\text{Hf}(t)$  between -3.4 and -7.6.

Analysis	Common $^{206}\text{Pb}$ (%)	U (ppm)	Th (ppm)	Th/U	Radiogenic ratios						Age (Ma)				Disc (%)	
					$^{207}\text{Pb}/^{235}\text{U}$	$\sigma$	$^{206}\text{Pb}/^{238}\text{U}$	$\sigma$	$\rho$	$^{207}\text{Pb}/^{206}\text{Pb}$	$\sigma$	$^{206}\text{Pb}/^{238}\text{U}$	$\sigma$	$^{207}\text{Pb}/^{206}\text{Pb}$	$\sigma$	
L20-34	1.02	1590	330	0.207	0.3450	0.0117	0.0468	0.0007	0.38	0.0534	0.0020	295	4	347	85	18
L20-35	0.19	330	281	0.851	5.5353	0.1042	0.3311	0.0043	0.36	0.1213	0.0023	1844	21	1975	34	7
L20-36	0	245	141	0.577	0.3577	0.0082	0.0480	0.0007	0.29	0.0540	0.0012	302	4	371	53	23
L24-1	0	635	318	0.500	0.3596	0.0062	0.0483	0.0006	0.44	0.0540	0.0009	304	4	372	38	22
L24-2	0	291	226	0.777	0.3720	0.0091	0.0479	0.0007	0.32	0.0563	0.0014	302	4	464	55	54
L24-3	0	1088	50	0.046	0.7040	0.0196	0.0837	0.0014	0.33	0.0610	0.0017	518	8	641	60	24
L24-4C	0	339	174	0.513	0.7413	0.0162	0.0891	0.0011	0.2	0.0604	0.0014	550	7	618	50	12
L24-4R	0	281	166	0.593	0.3788	0.0103	0.0499	0.0008	0.31	0.0550	0.0015	314	5	414	62	32
L24-5	0.39	113	73	0.646	5.2215	0.0922	0.3168	0.0038	0.29	0.1196	0.0022	1774	19	1950	33	10
L24-6	0	490	165	0.336	0.3510	0.0073	0.0481	0.0007	0.39	0.0529	0.0011	303	4	324	46	7
L24-9	0	539	272	0.505	0.7521	0.0117	0.0912	0.0011	0.44	0.0598	0.0009	563	7	597	33	6
L24-10	0	154	136	0.879	0.3634	0.0084	0.0494	0.0007	0.28	0.0534	0.0012	311	4	344	53	11
L24-11	-0.16	328	209	0.637	0.9244	0.0140	0.1058	0.0013	0.42	0.0634	0.0009	648	7	721	32	11
L24-12	0	116	54	0.470	1.3287	0.0207	0.1405	0.0016	0.34	0.0686	0.0011	847	9	888	34	5
L24-13	0.43	2539	146	0.057	0.3778	0.0116	0.0488	0.0008	0.26	0.0561	0.0019	307	5	457	78	49
L24-16	0.1	485	241	0.497	0.3776	0.0062	0.0489	0.0006	0.33	0.0560	0.0009	308	3	452	38	47
L24-17	0	185	144	0.778	0.3632	0.0156	0.0487	0.0009	0.16	0.0541	0.0024	306	6	376	101	23
L24-19	0	233	212	0.910	0.3538	0.0090	0.0477	0.0007	0.29	0.0538	0.0014	301	4	362	58	20
L24-20	0	218	146	0.668	0.3579	0.0110	0.0484	0.0008	0.22	0.0536	0.0017	305	5	355	72	16
L24-32	0	320	159	0.496	0.7701	0.0148	0.0935	0.0013	0.41	0.0598	0.0011	576	7	595	41	3
L24-33	0	272	163	0.597	1.0815	0.0183	0.1210	0.0015	0.38	0.0648	0.0011	736	8	769	36	4
L30-21	0	306	240	0.784	0.3597	0.0092	0.0481	0.0007	0.3	0.0542	0.0014	303	4	380	58	25
L30-22	0	920	63	0.068	0.8833	0.0264	0.1024	0.0018	0.29	0.0626	0.0019	629	10	694	65	10
L30-23	-0.44	672	344	0.512	0.3666	0.0080	0.0481	0.0007	0.37	0.0553	0.0012	303	4	423	48	40
L30-24	0	925	99	0.107	0.5643	0.0081	0.0717	0.0009	0.48	0.0571	0.0008	447	5	494	30	11
L30-25	0	2028	2046	1.009	0.8096	0.0148	0.0962	0.0013	0.47	0.0610	0.0010	592	8	641	37	8
L30-26	0	542	166	0.307	0.3563	0.0080	0.0480	0.0007	0.34	0.0539	0.0012	302	4	366	51	21
L30-27	0	440	311	0.709	0.3534	0.0069	0.0479	0.0006	0.37	0.0535	0.0010	301	4	351	44	17
L30-28	0	176	342	1.944	1.8804	0.0465	0.1819	0.0024	0.15	0.0750	0.0020	1078	13	1068	54	-1
L30-29	-0.38	2448	2228	0.910	0.3715	0.0075	0.0479	0.0007	0.41	0.0563	0.0011	301	4	463	44	54
L30-30	0.83	9542	250	0.026	0.3463	0.0078	0.0467	0.0006	0.35	0.0538	0.0014	294	4	361	61	23
L30-31	0	591	618	1.045	0.3494	0.0091	0.0475	0.0007	0.3	0.0534	0.0014	299	4	344	60	15

Table 5.- U-Pb LA-ICPMS data of zircons from the Logrosán granite

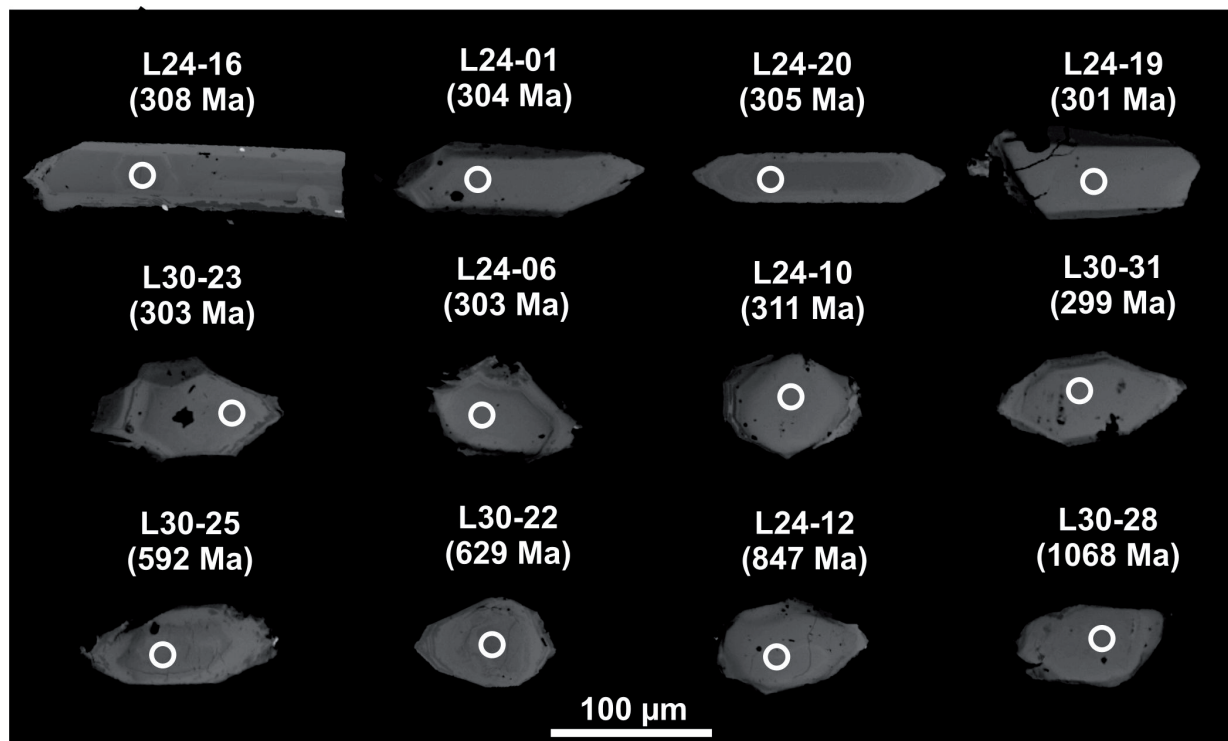


Fig. 6.- Back-scattered electron (BSE) images of representative zircons from the Logrosán granite. Spot numbers and ages are listed in Table 5.

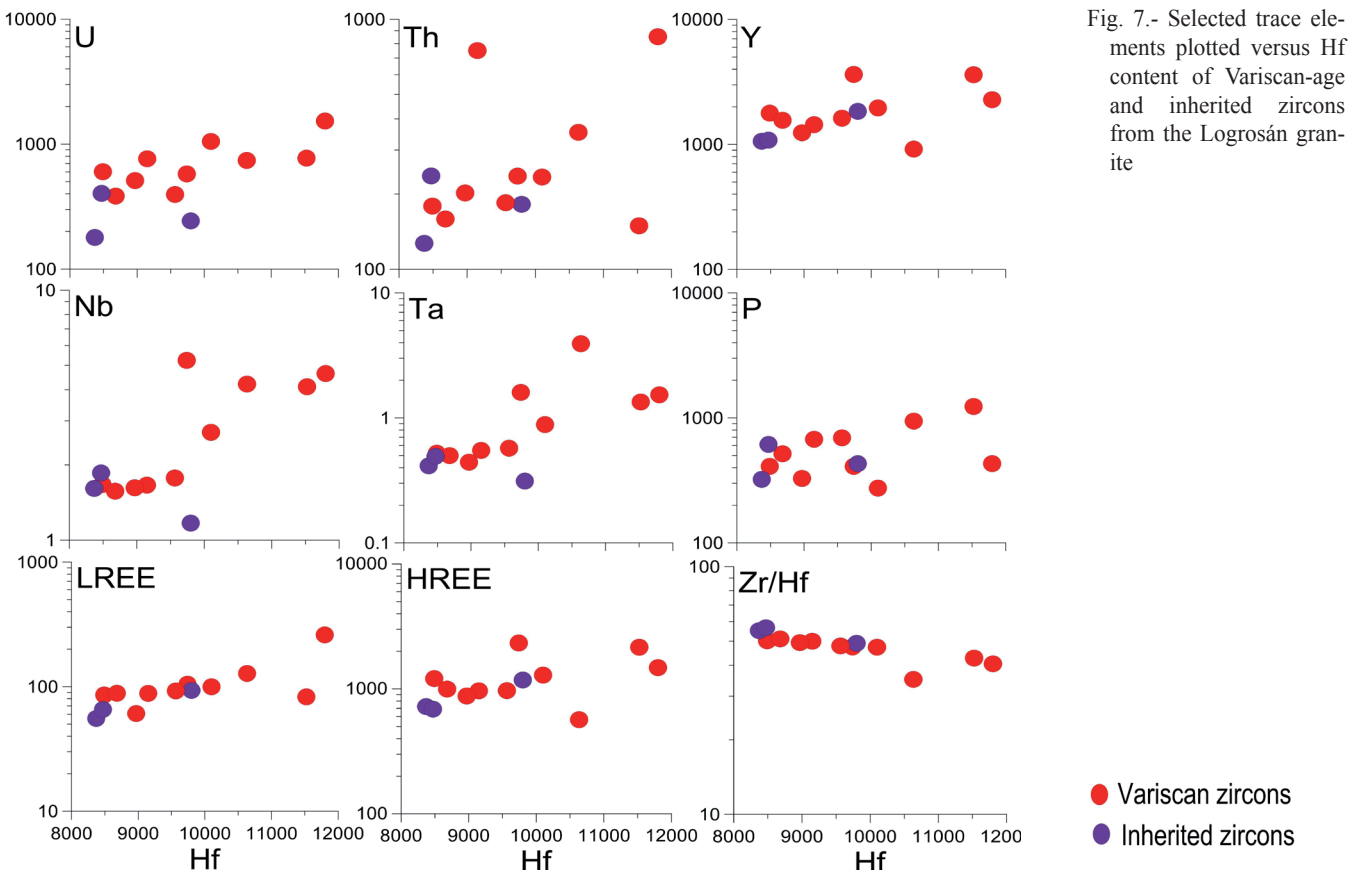


Fig. 7.- Selected trace elements plotted versus Hf content of Variscan-age and inherited zircons from the Logrosán granite

### 5.7. Zircon saturation and Ti-in-zircon thermometries

Zircon saturation thermometry has been calculated based on the relationship between zircon solubility, temperature, and major element composition of the melt (Watson and Harrison, 1983). Zircon saturation thermometry of the Logrosán granite ranges from 699°C to 777°C and yields an average temperature of 742°C (Table 1). Apparent temperatures for zircon crystallization have been also estimated using the Ti-in-zircon thermometer (Ferry and Watson, 2007). The Logrosán granite petrography suggests simultaneous crystallization of quartz, zircon and ilmenite, and thus  $a\text{SiO}_2 = 1$  and  $a\text{TiO}_2 < 1$ . An  $a(\text{TiO}_2)$  value of 0.6 based on the presence of ilmenite has been assumed. This would lead to underestimation of zircon crystallization temperatures by  $\leq 50$  °C (Watson and Harrison, 2005). Ti-in-zircon thermometry yields values from 744°C to 1024°C with an average temperature of 836°C (Table 3), these values are markedly higher than the ones obtained by zircon saturation thermometry.

## 6. Discussion

### 6.1. Granite fractional crystallization

The whole-rock geochemistry described above provides no evidence for a unique fractional crystallization trend to link the Main granite suite with the Evolved leucogranite Units. Hence, the Main and the Evolved Units are not re-

lated by simple crystal fractionation. Sequential restite fractionation can be dismissed as mafic xenoliths are absent in the Logrosán granite and most elements do not vary linearly with  $\text{SiO}_2$  contents (Chappell *et al.*, 1987). The low Ba and Sr contents together with high Rb concentrations found in the granites suggest that they have undergone some fractional crystallization (Breaks and Moore, 1992), which is consistent with a cupola stockwork scenario. Source-rock heterogeneities could explain the compositional evolution of the Logrosán granite since a significant number of major and trace elements do not show any linear correlations (Fig. 3). Moreover, the great variability in the whole-rock initial Sr isotopic ratios ( $^{87}\text{Sr}/^{86}\text{Sr}$ : 0.7125-0.7286) and the Hf-isotope composition of the Variscan-age zircons from the Logrosán granite (from +5.7 to -10.5) indicates a heterogeneous magmatic system. The variation of more than 15 εHf units (Table 6) is the maximum range obtained in zircons from the Iberian Variscan granites (Villaseca *et al.*, 2012; Teixeira *et al.*, 2011). Besides, the lack of a single evolutionary path in terms of Sr, Ba, Rb, Eu and CaO between the Main and Evolved Units indicates that fractional crystallization of plagioclase and K-feldspar did not occur in a simple closed magmatic system. Magmatic recharge from a deeper and chemically heterogeneous magma reservoir could produce the more residual and evolved granites of the Logrosán cupola. Thus a complex multi-pulse granite system inefficiently mixed, formed by isotopically heterogeneous fractionated magmas that episodically replenish the Logrosán cupola is more likely

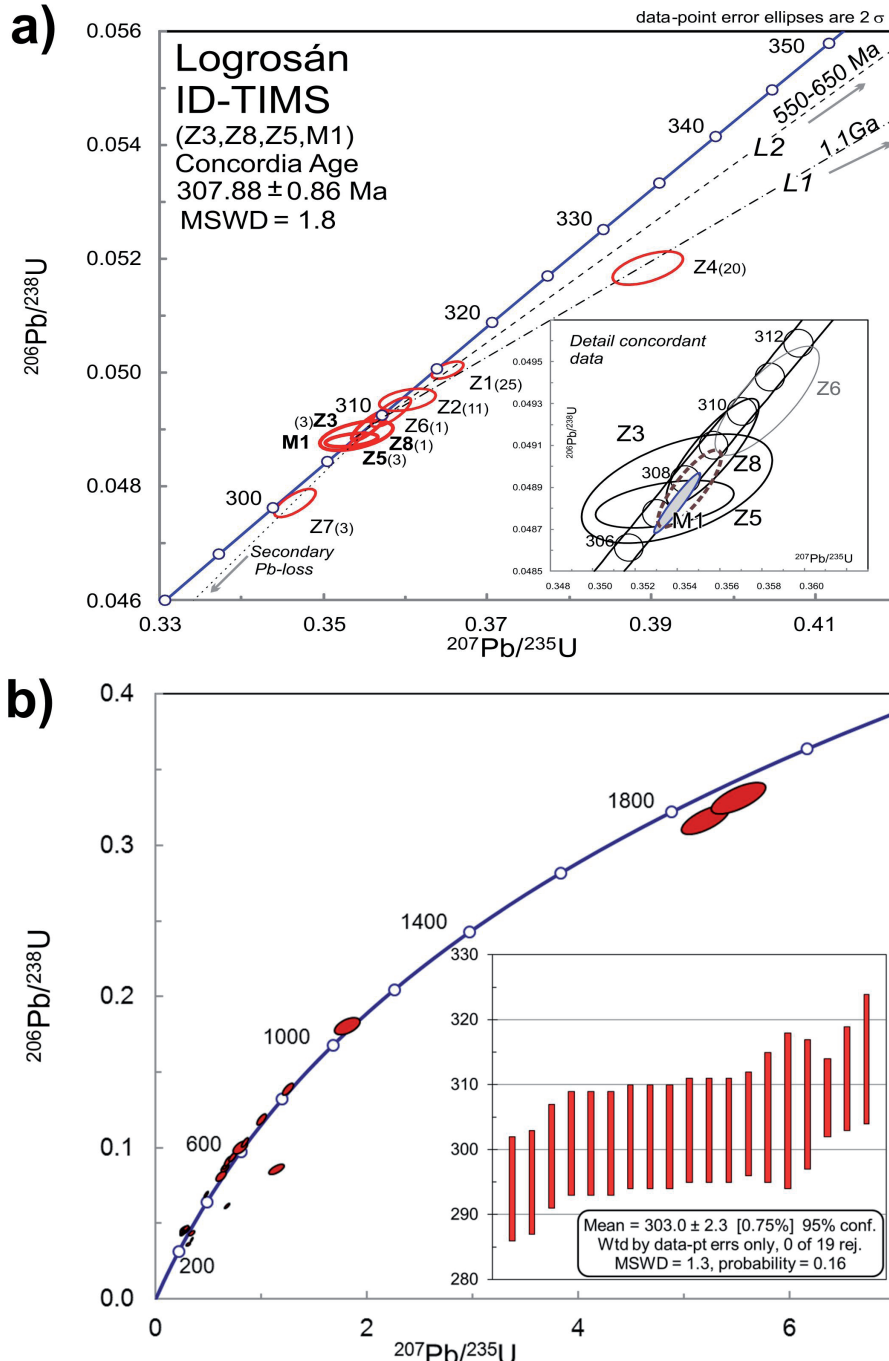


Fig. 8.- (a) Concordia diagram of the ID-TIMS data. Zircon (Z) and monazite (M) fractions, respectively; within brackets, number of crystals in each fraction. (b) U-Pb LA-ICPMS data showing weighted average  $^{206}\text{Pb}/^{238}\text{U}$  ages and concordia plots.

than a single magma batch following closed *in situ* fractional crystallization processes.

#### 6.2. Zircon saturation and Ti-in-zircon thermometries

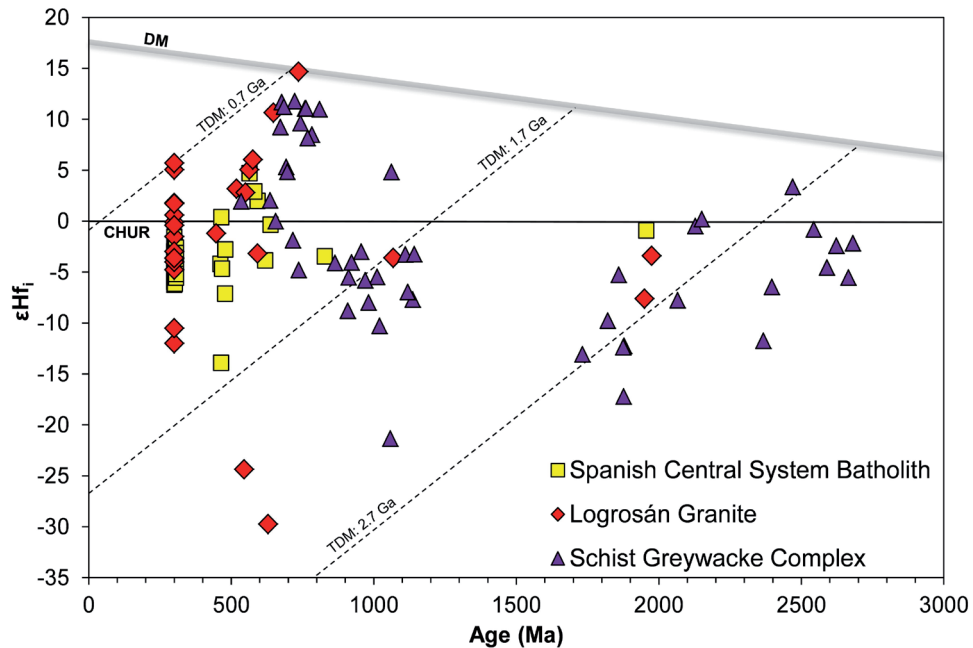
The average temperatures obtained for the Logrosán Variscan-age zircon crystallization is 836 °C, similar to other temperature estimates on S-type granites of the Central Iberian Zone (788 to 844°C after Orejana *et al.*, 2012). Lower temperature estimates (699–777 °C, Table 1) have been obtained based on whole-rock zircon saturation. The average whole-rock zircon saturation temperature (742°C) is below the average Ti-in zircon temperature (836°C) for the Logrosán granite. Granitoids rich in zircon inheritances are probably

undersaturated with respect to zircon at the source and consequently their calculated zircon saturation temperatures are most likely underestimations of the actual temperature of crystallization (Miller *et al.*, 2003). The zircon inheritances of the Logrosán granite may yield unrealistic zircon saturation temperatures. Hence, the average Ti-in-zircon temperature (836°C) provides a better estimation of the temperature of the magma from which the zircon crystallized.

#### 6.3. Inheritances and source constraints

Mineralogical and geochemical features of the Logrosán granite (e.g., high peraluminosity and low CaO contents) and the absence of mafic microgranular enclaves suggest a crus-

Fig. 9.- Initial epsilon Hf vs. U-Pb age plot of the zircons from the Logrosán granite. Data from the SGC (represented by the Sabugal sample from Teixeira *et al.*, 2011) and the Spanish Central System granitoids (Villaseca *et al.*, 2012) are given for comparison. Dotted lines indicate the crustal evolution paths at 0.7 Ga ( $^{176}\text{Lu}/^{177}\text{Hf} = 0.0010$ ), 1.7 Ga ( $^{176}\text{Lu}/^{177}\text{Hf} = 0.0013$ ) and 2.7 Ga ( $^{176}\text{Lu}/^{177}\text{Hf} = 0.0006$ ).



tal-derived melt origin with a major contribution of aluminous metasedimentary sources (Dias *et al.*, 2002; Chappell *et al.*, 1991). Likewise, high whole rock  $\delta^{18}\text{O}$  values point to an  $\delta^{18}\text{O}$ -enriched sedimentary or metasedimentary protolith. Perphosphorous character may be inherited from a P-rich source (Villaseca *et al.*, 2008; Rodríguez-Alonso *et al.*, 2004) as indicated in other P-rich granites of the area (Antunes *et al.*, 2008; Villaseca *et al.*, 2008; Ramírez and Menéndez, 1999). This P-rich character is also consistent with the presence of phosphate mineralizations surrounding the granite and with dispersed phosphate mineralizations in the regional Schist Greywacke Complex (Vindel *et al.*, 2014).

Zircons from the Logrosán granite have Zr/Hf ratios ranging 41-55 with an average value of 48. According to Pupin (2000), the estimated signature of zircon from the continental crust is 36-45. However, Pérez-Soba *et al.* (2007) estimated the Zr/Hf ratios of zircons from migmatites and augen orthogneisses of the Spanish Central System and suggested a slightly higher range (Zr/Hf = 36-56) for pure crustal signatures. Hence Zr/Hf ratios of the Logrosán zircon fit well with crustal signatures. It is expected that the Zr/Hf ratio in a single magma series should be approximately constant (Wang *et al.*, 2010). Therefore, the wide range of Zr/Hf values for such a small granitic body may indicate not only a different degree of differentiation but also a participation of several magma inputs.

The high initial  $^{87}\text{Sr}/^{86}\text{Sr}$  ratios of the Logrosán samples are attributed to a significant participation of the Sr derived from crustal material as established for similar granitoids of the CIZ (Ruiz *et al.*, 2008; Castro *et al.*, 1999; Villaseca *et al.*, 1998). Variability in  $^{87}\text{Sr}/^{86}\text{Sr}$  data for the Logrosán granite (Fig. 5) may well indicate an origin by partial melting of a compositionally heterogeneous continental crust. The  $^{87}\text{Sr}/^{86}\text{Sr}$  ratios of the Logrosán granite plot in an intermediate space in the Sr-Nd isotopic field drawn by other monzogranites and leu-

cogranites from the Central Extremadura Batholith. The large variability in  $^{87}\text{Sr}/^{86}\text{Sr}$  data at almost constant  $\epsilon\text{Nd}$  values can hardly indicate mixing of different proportions of mantle-derived magmas with crustal sources (Castro *et al.*, 1999). The low negative initial Nd isotope ratios of the Logrosán granite (around -4.2), typical of other Central Extremadura Batholith granites (e.g., Castelo Branco, Antunes *et al.*, 2008; Alburquerque, González Menéndez and Bea, 2004; Montes de Toledo, Villaseca *et al.*, 2008), contrasts with other S-type granites from northern areas of the CIZ (Fig. 5). The metasediments of the SGC also show low Nd isotope signatures (at Variscan times) and might be the most appropriate protolith of the Logrosán granite (Fig. 5).

Inherited zircons in the Logrosán granite define an age range of *ca.* 447-1975 Ma displaying predominant Neoproterozoic populations (Table 5). Despite the limited dataset (13 inherited zircons), it is still possible to distinguish two main groups: (1) Cambro-Ordovician and Neoproterozoic ages and (2) Meso- and Paleoproterozoic ages (Fig. 10). The first group of inheritance (Early Paleozoic and Neoproterozoic) is the most abundant and fits well with materials derived from the Cadomian orogeny. The minor amount of Mesoproterozoic zircon inheritances and the distribution of Nd and Hf model ages around  $1.45 \pm 0.2$  Ga, either in Variscan granites and Neoproterozoic metasediments, have been attributed to the Saharan and Arabian-Nubian shields as possible supplying provinces for the Central Iberian Zone (e.g., Pereira *et al.*, 2012; Villaseca *et al.*, 2011; Bea *et al.*, 2010; Henry *et al.*, 2009). The only Ordovician age (*ca.* 447 Ma) could be related to the Ordovician magmatism described along the Central Iberian Zone (e.g., Rubio-Ordóñez *et al.*, 2012; Neiva *et al.*, 2009; Solá *et al.*, 2008; Bea *et al.*, 2007). In general, the probability density curve of the Logrosán granite inheritances shows a broad overlap with the zircon U-Pb age distribution previously reported for the Schist Greywacke Complex ages

Sample	$^{176}\text{Hf}/^{177}\text{Hf}$	1SE	$^{176}\text{Lu}/^{177}\text{Hf}$	$^{176}\text{Yb}/^{177}\text{Hf}$	Age (Ma)	$\text{Hf}_i$	$\epsilon\text{Hf}$	1SE	$T_{\text{DM}}(\text{Ga})$	$T_{\text{DM2}}(\text{Ga})$
L24-1	0.282745	0.000039	0.0011	0.0295	308	0.282739	5.0	1.4	0.72	0.98
L24-2	0.282761	0.000059	0.0006	0.0166	308	0.282758	5.7	2.1	0.69	0.93
L24-6	0.282555	0.000057	0.0003	0.0087	308	0.282553	-1.5	2.0	0.97	1.39
L24-10	0.282466	0.000052	0.0008	0.0221	308	0.282462	-4.8	1.8	1.11	1.60
L24-16	0.282516	0.000041	0.0006	0.0171	308	0.282512	-3.0	1.5	1.03	1.49
L24-17	0.282496	0.000053	0.0005	0.0146	308	0.282493	-3.7	1.9	1.06	1.53
L24-19	0.282653	0.000029	0.0011	0.0318	308	0.282647	1.8	1.0	0.85	1.18
L24-20	0.282601	0.000033	0.0013	0.0359	308	0.282594	-0.1	1.2	0.93	1.30
L24-21	0.282304	0.000140	0.0008	0.0219	308	0.282299	-10.5	5.0	1.33	1.96
L24-23	0.282488	0.000035	0.0008	0.0239	308	0.282483	-4.0	1.2	1.08	1.55
L24-26	0.282614	0.000032	0.0002	0.0059	308	0.282613	0.6	1.1	0.88	1.26
L24-27	0.282591	0.000035	0.0011	0.0313	308	0.282585	-0.4	1.2	0.94	1.32
L24-31	0.282502	0.000160	0.0014	0.0378	308	0.282494	-3.6	5.7	1.07	1.53
L24-36	0.282651	0.000050	0.0010	0.0295	308	0.282645	1.7	1.8	0.85	1.19
L24-24	0.282489	0.000110	0.0023	0.0654	447	0.282469	-1.2	3.9	1.12	1.49
L24-3	0.282557	0.000046	0.0009	0.0214	518	0.282549	3.2	1.6	0.98	1.27
L24-7	0.281758	0.000052	0.0004	0.0103	545	0.281753	-24.4	1.8	2.07	3.02
L24-4	0.282528	0.000048	0.0010	0.0263	550	0.282518	2.8	1.7	1.03	1.32
L24-9	0.282586	0.000036	0.0012	0.0299	563	0.282573	5.1	1.3	0.95	1.18
L24-32	0.28261	0.000049	0.0016	0.0425	576	0.282592	6.0	1.7	0.93	1.13
L24-25	0.282338	0.000032	0.0014	0.0400	592	0.282322	-3.2	1.1	1.31	1.73
L24-22	0.281564	0.000069	0.0013	0.0314	629	0.281549	-29.7	2.5	2.38	3.42
L24-11	0.282687	0.000034	0.0008	0.0217	648	0.282677	10.6	1.2	0.80	0.89
L24-33	0.282749	0.000040	0.0010	0.0237	736	0.282735	14.7	1.4	0.71	0.70
L24-12	0.282264	0.000057	0.0011	0.0330	847	0.282246	-0.2	2.0	1.40	1.74
L24-28	0.282034	0.000032	0.0013	0.0352	1068	0.282007	-3.6	1.1	1.73	2.14
L24-05	0.28134	0.000051	0.0004	0.0097	1950	0.281326	-7.6	1.8	2.63	3.09
L24-35	0.281449	0.000057	0.0005	0.0140	1975	0.281428	-3.4	2.0	2.49	2.84

Table 6.- Lu-Hf LA-MC-ICPMS data of zircons from the Logrosán granite

(Talavera *et al.*, 2012; Teixeira *et al.*, 2011; Gutiérrez-Alonso *et al.*, 2003) (Fig. 10). This comparison again points to the Schist Greywacke Complex as the most probable protolith of the Logrosán granite.

Magmatic zircons from the Logrosán granite have a significant wide range of  $\epsilon\text{Hf}_{(t)}$  values showing variations up to 15  $\epsilon\text{Hf}$  units, similar to those observed in samples of Variscan S-type granites from northern Portugal (Teixeira *et al.*, 2011). The large range of negative  $\epsilon\text{Hf}_{(t)}$  values is in agreement with the S-type nature of the granite but there is also a significant proportion of positive  $\epsilon\text{Hf}_{(t)}$  values (Fig. 9). The large range of negative  $\epsilon\text{Hf}_{(t)}$  values denotes an origin by partial melting of heterogeneous crustal sources or by crustal contamination of a mantle-derived parental magma as proposed for other Variscan S-type granites from the Central Iberian Zone (Teixeira *et al.*, 2011; Neiva *et al.*, 2013). Although positive  $\epsilon\text{Hf}_{(t)}$  values tend to be interpreted as mantle-derived, this cannot be easily applied to the Logrosán granite. The absence of coeval mafic magmatism and the clearly peraluminous and perphosphorous character of the Logrosán cupola is more in agreement with the involvement of recycled juvenile material in the genesis of this granite. From this prospective,  $\epsilon\text{Hf}$  values of Neoproterozoic zircons from the SGC metasediments (sample from Sabugal area, spots 21 and 70 of Teixeira *et al.*, 2011), recalculated at the age of the Logrosán granite emplacement, yield positive values (up to +4.5) that overlap with those found in Variscan-age zircons from the Logrosán granite. Moreover, some inherited Neoproterozoic zircons within the Logrosán granite show strong positive  $\epsilon\text{Hf}_{(t)}$  values (up to +14.7, e.g. L24-33, Table 6) similar to zircon populations found in metasediments from the SGC (up to +11.7,

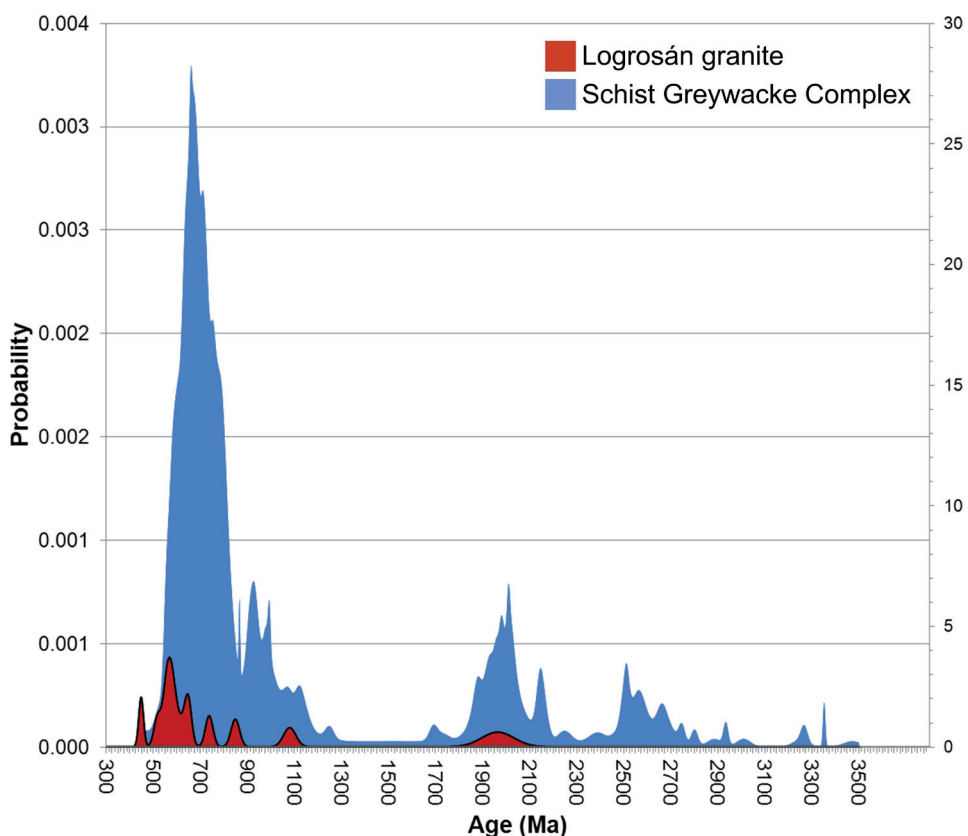
spot Malcl-21 of Teixeira *et al.*, 2011). Such correlation reinforces the genetic relationship with this probable protolith (Fig. 9) and is in agreement with the presence of a recycled mantle-derived component in the granite crustal source.

#### 6.4. Geochronological comparison

Widespread granite generation occurred across the Central Iberian Zone over 325-300 Ma time interval (e.g., Dias *et al.*, 1998; Fernández Suárez *et al.*, 2000; Bea *et al.*, 2003; Orejana *et al.*, 2012). Most of the felsic magmatism in the CIZ is syn-to post-tectonic with respect to the last ductile deformation phase ( $D_3$ ) (Dias *et al.*, 1998) with three peaks at 320 (mainly syn- $D_3$  leucogranites of Galicia and northern Portugal), 308-306 and 301 Ma (Orejana *et al.*, 2012; Teixeira *et al.*, 2011; Fernández-Suárez *et al.*, 2000; Dias *et al.*, 1998). The U-Pb results presented here indicate that the Logrosán intrusion occurred at ca. 308 Ma, thus in a post-tectonic Variscan stage.

The comparison of the ages of the granites from the southern CIZ (those of the Central Extremadura Batholith) and the Logrosán granite shows a good overlap: 310 Ma for Castelo Branco (Antunes *et al.*, 2008), 308 Ma for Nisa-Alburquerque (Solá *et al.*, 2009), 314-298 Ma for the Montes de Toledo (Orejana *et al.*, 2011), and 309 Ma for the Cabeza de Araya and Trujillo plutons (Gutiérrez-Alonso *et al.*, 2011). They are also similar in age to the emplacement of the Los Pedroches batholith (314-304 Ma, Carracedo *et al.*, 2009) located in the southern edge of the CIZ and to the age range of emplacement of the Spanish Central System batholith (311-298 Ma, Orejana *et al.*, 2012; Díaz-Alvarado *et al.*, 2011; Zeck *et al.*, 2007; Bea *et al.*, 2003). These similarities in age indicate that

Fig. 10.- Relative probability plots of the inherited zircon U-Pb ages of the Logrosán granite (dark gray fields) compared to the data available of the CIZ metasediments of the Schist Greywacke Complex (light gray fields): samples ZD1 and ZD2 (Gutiérrez-Alonso *et al.*, 2003), sample of the Sabugal area (Teixeira *et al.*, 2011), samples PNC1 and PNC2 (Pereira *et al.*, 2012), and sample Ctc67 (Talavera *et al.*, 2012).



granite batholiths and plutons from the Spanish Central System and the southern CIZ are practically coeval.

## 7. Conclusions

The Logrosán cupola is a felsic, perphosphoric and strongly peraluminous (ASI=1.2-2) tin-granite (Sn=11-67 ppm). Two distinct units can be distinguished using field, petrographic and geochemical evidences: (1) a coarse-grained monzogranite (Main Unit) and (2) highly fractionated leucogranite bodies mostly concentrated on the top of the pluton (Evolved Units). U-Pb zircon analyses yield a concordia age of 307.88 ± 0.86 Ma which is considered the age of the emplacement of the Logrosán granite, coeval with other post-Variscan granites of the Central Iberian Zone. The Ti-in-zircon thermometry provides an average estimated temperature of 836°C for the parental magma. The whole-rock geochemistry does not indicate that simple fractional crystallization may produce both the Main and the Evolved granite suites. Complex Sr, Ba, Rb, Eu and CaO trends rather suggest inputs of different felsic magma batches from a deep magma reservoir. The integration of whole-rock geochemistry with O, Sr, Nd and Hf isotopic signatures suggests that the Logrosán granite is the result of partial melting of heterogeneous metasedimentary materials. And finally, zircon inheritance (mostly Neoproterozoic zircons) combined with the metasedimentary nature of the proposed protolith, allow to suggest that the Schist Greywacke Complex is the most appropriated source of the Logrosán granitic magma.

## Acknowledgments

This work was supported by the projects CGL2012-32822 (Economy and Competitiveness Spanish Office) and 910492 (Complutense University), and the grant for C.Villaseca from Fundación CajaMadrid. E. Chicharro would like to express her gratitude to Dr. Teresa E. Jeffries, from the Natural History Museum of London, for the provision of the analytical facilities and her assistance with the laser ablation technique. C. Villaseca also thanks the opportunity to undertake the analytical work in the Geochemical Analysis unit at GEMOC, at Macquarie University. We acknowledge Norman Pearson and Will Powell for their assistance with the LA-ICPMS analyses. PVV thanks funding from grant CGL2008-05952-CO2-O2/BTE. Thanks are also given to Dr. Teresa Ubide, one anonymous reviewer and the editors whose thorough and helpful comments greatly improved the quality of the manuscript. Grateful thanks to Dr. Clemente Recio for carrying out the stable isotope analysis. This is contribution 464 from the ARC Centre of Excellence for Core to Crust Fluid Systems (<http://www.ccfs.mq.edu.au>) and 941 in the GEMOC Key Centre (<http://www.gemoc.mq.edu.au>).

## References

- Ábalos, A., Carreras, J., Druguet, E., Escuder, J., Gómez Pugnaire, M.T., Lorenzo, S. (2002): Variscan and Pre-Variscan Tectonics. In: W. Gibbons and M.T. Moreno (ed.), *The Geology of Spain*. Geological Society of London, London, pp. 155-183.

- Andersen, T., Griffin, W., Pearson, N. (2002): Crustal evolution in the SW part of the Baltic Shield: the Hf isotope evidence. *Journal of Petrology* 43, 1725-1747. doi:10.1093/petrology/43.9.1725
- Antunes, I., Neiva, A., Silva, M., Corfu, F. (2008): Geochemistry of S-type granitic rocks from the reversely zoned Castelo Branco pluton (central Portugal). *Lithos* 103, 445-465. doi:10.1016/j.lithos.2007.10.003
- Bea, F., Montero, P., González-Lodeiro, F., Talavera, C. (2007): Zircon inheritance reveals exceptionally fast crustal magma generation processes in Central Iberia during the Cambro-Ordovician. *Journal of Petrology* 48, 2327-2339. doi:10.1093/petrology/egm061
- Bea, F., Montero, P., Talavera, C., Abu Anbar, M., Scarrow, J. H., Molina, J. F., Moreno, J. A. (2010): The palaeogeographic position of Central Iberia in Gondwana during the Ordovician: evidence from zircon chronology and Nd isotopes. *Terra Nova* 22, 341-346. doi:10.1111/j.1365-3121.2010.00957.x
- Bea, F., Montero, P., Zinger, T. (2003): The nature, origin, and thermal influence of the granite source layer of Central Iberia. *The Journal of Geology* 111, 579-595. doi:10.1086/376767
- Beetsma, J.J. (1995): *The late Proterozoic/Paleozoic and Hercynian crustal evolution of the Iberian Massif, N Portugal, as traced by geochemistry and Sr-Nd-Pb isotope systematics of pre-Hercynian terrigenous sediments and Hercynian granitoids*, PhD Thesis, Vrije Universiteit, Amsterdam, 223 p.
- Belousova, E., Griffin, W.L., O'Reilly, S.Y., Fisher, N. (2002): Igneous zircon: trace element composition as an indicator of source rock type. *Contributions to Mineralogy and Petrology* 143, 602-622. doi:10.1007/s00410-002-0364-7
- Black, L., Gulson, B. (1978): The age of the mud tank carbonatite, strangways range, northern territory. *BMR Journal of Australian Geology and Geophysics* 3, 227-232.
- Borthwick, J., Harmon, R.S. (1982): A note regarding  $\text{ClF}_3$  as an alternative to  $\text{BrF}_5$  for oxygen isotope analysis. *Geochimica et Cosmochimica Acta* 46, 1665-1668. doi:10.1016/0016-7037(82)90321-0
- Bouvier, A., Vervoort, J.D., Patchett, P.J. (2008): The Lu-Hf and Sm-Nd isotopic composition of CHUR: constraints from unequilibrated chondrites and implications for the bulk composition of terrestrial planets. *Earth and Planetary Science Letters* 273, 48-57. doi:10.1016/j.epsl.2008.06.010
- Breaks, F.W., Moore, J.M. (1992): The Ghost Lake Batholith, Superior Province of northwestern Ontario; a fertile, S-type, peraluminous granite-rare-element pegmatite system. *The Canadian Mineralogist* 30, 835-875.
- Carracedo, M., Paquette, J.L., Alonso Olazabal, A., Santos Zalduogui, J.F., García de Madinabeitia, S., Tiepolo, M., Gil Ibarguchi, J.I. (2009): U-Pb dating of granodiorite and granite units of the Los Pedroches batholith. Implications for geodynamic models of the southern Central Iberian Zone (Iberian Massif). *International Journal of Earth Sciences* 98, 1609-1624. doi:10.1007/s00531-008-0317-0
- Castro, A. (1985): The Central Extremadure Batholith - Geotectonic implications (European Hercynian Belt) - An outlet. *Tectonophysics* 120, 57-68. doi:10.1016/0040-1951(85)90086-1
- Castro, A., Patiño, E., Corretgé, L.G., De La Rosa, J., El-Biad, M., El-Hmidi, H. (1999): Origin of peraluminous granites and granodiorites, Iberian massif, Spain: an experimental test of granite petrogenesis. *Contributions to Mineralogy and Petrology* 135, 255-276. doi:10.1007/s004100050511
- Chappell, B., White, A., Williams, I. (1991): A transverse section through granites of the Lachlan Fold Belt. *Second Hutton Symposium on Granites and Related Rocks*, Canberra, pp. 1-125.
- Chappell, B., White, A., Wyborn, D. (1987): The importance of residual source material (restite) in granite petrogenesis. *Journal of Petrology* 28, 1111-1138. doi:10.1093/petrology/28.6.1111
- Chicharro, E., Villaseca, C., López-García, J.A., Oyarzun, R. (2011): Caracterización mineral del granito peraluminoso de Logrosán (Cáceres, España). *Geogaceta* 50, 71-74.
- Clayton R. N., Mayeda T. K. (1963): The use of bromine pentafluoride in the extraction of oxygen from oxides and silicates for isotopic analysis. *Geochimica et Cosmochimica Acta* 27, 43-52. doi:10.1016/0016-7037(63)90071-1
- Dallmeyer, R.D., Martínez Catalán, J.R., Arenas, R., Gil-Ibarguchi, J.I., Gutiérrez-Alonso, G., Farias, P., Bastida, F., Aller, J. (1997): Diachronous Variscan tectonothermal activity in the NW Iberian Massif: Evidence from  $^{40}\text{Ar}/^{39}\text{Ar}$  dating of regional fabrics. *Tectonophysics* 277, 307-377. doi:10.1016/S0040-1951(97)00035-8
- Dias, G., Leterrier, J., Mendes, A., Simões, P., Bertrand, J. (1998): U-Pb zircon and monazite geochronology of post-collisional Hercynian granitoids from the Central Iberian Zone (Northern Portugal). *Lithos* 45, 349-369. doi:10.1016/S0024-4937(98)00039-5
- Dias, G., Simões, P., Ferreira, N., Leterrier, J. (2002): Mantle and crustal sources in the genesis of late-Hercynian granitoids (NW Portugal): geochemical and Sr-Nd isotopic constraints. *Gondwana Research* 5, 287-305. doi:10.1016/S1342-937X(05)70724-3
- Díaz-Alvarado, J., Castro, A., Fernández, C., Moreno-Ventas, I. (2011): Assessing bulk assimilation in cordierite-bearing granitoids from the Central System Batholith, Spain; experimental, geochemical and geochronological constraints. *Journal of Petrology*, 52, 223-256. doi:10.1093/petrology/eqq078
- Díez Balda, M.A., Martínez Catalán, J.R., Ayarza, P. (1995): Syn-collisional extensional collapse parallel to the orogenic trend in a domain of steep tectonics: the Salamanca detachment zone (Central Iberian Zone, Spain). *Journal of Structural Geology* 17, 163-182. doi:10.1016/0191-8141(94)E0042-W
- Fernández-Suárez, J., Dunning, G., Jenner, G., Gutiérrez-Alonso, G. (2000): Variscan collisional magmatism and deformation in NW Iberia: constraints from U-Pb geochronology of granitoids. *Journal of the Geological Society* 157, 565-576. doi:10.1144/jgs.157.3.565
- Ferry, J., Watson, E. (2007): New thermodynamic models and revised calibrations for the Ti-in-zircon and Zr-in-rutile thermometers. *Contributions to Mineralogy and Petrology* 154, 429-437. doi:10.1007/s00410-007-0201-0
- Flinter, B. (1971): Tin in acid granitoids: a search for a geochemical scheme of mineral exploration. *Proceedings of the 3rd International Geochemical Exploration Symposium*, Toronto, pp. 323-330.
- Godfrey, J.D. (1962): The deuterium content of hydrous minerals from the east-central Sierra Nevada and Yosemite National Park. *Geochimica et Cosmochimica Acta* 26, 1215-1245. doi:10.1016/0016-7037(62)90053-4
- González Menéndez, L., Bea, F. (2004): Magmatismo de la zona Centroibérica: El batolito de Nisa-Alburquerque. In: J.A. Vera (ed.), *Geología de España*. SGE-IGME, Madrid, pp. 120-122.
- Griffin, W. L., Pearson, N. J., Belousova, E. A., Jackson, S. R., van Achterbergh, E., O'Reilly, S. Y., Shee, S. R. (2000): The Hf isotope composition of cratonic mantle: LAM-MC-ICPMS analysis of zircon megacrysts in kimberlites. *Geochimica et Cosmochimica Acta* 64, 133-147. doi:10.1016/S0016-7037(99)00343-9
- Griffin, W. L., Pearson, N. J., Belousova, E. A., Jackson, S. R., van Achterbergh, E., O'Reilly, S. Y., Shee, S. R. (2002): Zircon chemistry and magma mixing, SE China: in-situ analysis of Hf isotopes, Tonglu and Pingtan igneous complexes. *Lithos* 61, 237-269. doi:10.1016/S0024-4937(02)00082-8
- Griffin, W., Belousova, E., Shee, S., Pearson, N., O'Reilly, S. (2004): Archean crustal evolution in the northern Yilgarn Craton: U-Pb and Hf-isotope evidence from detrital zircons. *Precambrian Research* 131, 231-282. doi:10.1016/j.precamres.2003.12.011
- Gutiérrez-Alonso, G., Fernandez-Suarez J., Jeffries T.E., Jenner G.A.,

- Tubrett M.N., Cox R., Jackson S.E. (2003): Terrane accretion and dispersal in the northern Gondwana margin. An Early Paleozoic analogue of a long-lived active margin. *Tectonophysics* 365, 221-232. doi:10.1016/S0040-1951(03)00023-4
- Gutiérrez-Alonso, G., Fernández-Suárez, J., Jeffries, T.E., Johnston, S.T., Pastor-Galán, D., Murphy, J.B., Franco, M.P., Gonzalo, J.C. (2011): Diachronous post-orogenic magmatism within a developing orocline in Iberia, European Variscides. *Tectonics* 30, TC5008. doi:10.1029/2010TC002845
- Hanchar, J.M., Watson, E.B. (2003): Zircon saturation thermometry. *Reviews in Mineralogy and Geochemistry* 53, 89-112. doi:10.2113/0530089
- Henry, B., Liegeois, J.P., Nouar, O., Derder, M.E.M., Bayou, B., Bruguier, O., Ouabadi, A., Belhai, D., Amenna, M., Hemmi, A., Ayache, M. (2009): Repeated granitoid intrusions during the Neoproterozoic along the western boundary of the Saharan metacraton, Eastern Hoggar, Tuareg shield, Algeria: an AMS and U-Pb zircon age study. *Tectonophysics* 474, 417-434. doi:10.1016/j.tecto.2009.04.022
- Hoefs, J., Emmermann, R. (1983): The oxygen isotope composition of Hercynian granites and pre-Hercynian gneisses from the Schwarzwald, SW Germany. *Contributions to Mineralogy and Petrology* 83, 320-329. doi:10.1007/BF00371200
- Hoskin, P.W., Schaltegger, U. (2003): The composition of zircon and igneous and metamorphic petrogenesis. *Reviews in Mineralogy and Geochemistry* 53, 27-62. doi:10.2113/0530027
- Isachsen, C.E., Coleman, D.S. and Schmitz, M. (2007): PbMacDat program. Available at <http://www.earthtime.org>.
- Jaffey, A., Flynn, K., Glendenin, L., Bentley, W., Essling, A. (1971): Precision measurement of the half-lives and specific activities of  $U^{235}$  and  $U^{238}$ . *Physical Review C - Nuclear Physics* 4, 1889-1906. doi:10.1103/PhysRevC.4.1889
- Jenkin, G.R.T. (1988): *Stable isotope studies in the Caledonides of SW Connemara, Ireland*. PhD Thesis, University of Glasgow, Glasgow, UK.
- Julivert, M., Fontboté, J., Ribeiro, A., Conde, L. (1972): *Mapa Tectónico de la Península Ibérica Y Baleares, E. 1:1.000.000*. I.G.M.E., Madrid.
- Krogh, T.E. (1973): A low-contamination method for hydrothermal decomposition of zircon and extraction of U and Pb for isotopic age determinations. *Geochimica et Cosmochimica Acta* 37, 485-494. doi:10.1016/0016-7037(73)90213-5
- Krogh, T.E. (1982): Improved accuracy of U-Pb zircon ages by the creation of more concordant systems using an air abrasion technique. *Geochimica et Cosmochimica Acta* 46, 637-649. doi:10.1016/0016-7037(82)90165-X
- Liew, T., Hofmann, A. (1988): Precambrian crustal components, plutonic associations, plate environment of the Hercynian Fold Belt of central Europe: indications from a Nd and Sr isotopic study. *Contributions to Mineralogy and Petrology* 98, 129-138. doi:10.1007/BF00402106
- Linnen, R.L., Keppler, H. (2002): Melt composition control of Zr/Hf fractionation in magmatic processes. *Geochimica et Cosmochimica Acta* 66, 3293-3301. doi:10.1016/S0016-7037(02)00924-9
- Locutura, J., Alcalde, C., Boixereu, E., Florido, P., García Cortés, A., González, F. J., Gumi, P., Tornos, F., Urbano, R., Lopera, E., Sánchez, A., Bel-Lan, A., Fernández Leyva, C., Martínez, S., Pérez, F., Eguíluz, L., Alpategui, O. (2007): *Mapa Metalogenético de Extremadura E. 1:250.000*. I.G.M.E. - Junta de Extremadura, Madrid.
- López Plaza, M., Martínez Catalán, J.M. (1987): Síntesis estructural de los granitoides del Macizo Hespérico. In: F. Bea, A. Carnicer, J.C. Gonzalo, M. López Plaza, M.D. Rodríguez Alonso (eds.), *Geología de los granitoides y rocas asociadas del Macizo Hespérico*. Rueda, Madrid, pp. 195-220.
- López-Guijarro, R., Armendáriz, M., Fernández-Suárez, J., Quesada, C., Murphy, J.B., Pin, Ch., Bellido F. (2008): Ediacaran-Palaeozoic tectonic evolution of the Ossa Morena and Central Iberian zones (SW Iberia) as revealed by Sm-Nd isotope systematics. *Tectonophysics* 461, 202-214. doi:10.1016/j.tecto.2008.06.006
- López-Moro, F. J., López-Plaza, M., Romer, R. L. (2012): Generation and emplacement of shear-related highly mobile crustal melts: the synkinematic leucogranites from the Variscan Tormes Dome, Western Spain. *International Journal of Earth Sciences* 101, 1273-1298. doi:10.1007/s00531-011-0728-1
- Ludwig, K.R. (2003): User's manual for Isoplot 3.00: A geochronological toolkit for Microsoft Excel. Kenneth R. Ludwig.
- Martínez Catalán, J.R. (2011): Are the oroclines of the Variscan belt related to late Variscan strike-slip tectonics? *Terra Nova* 23, 241-247. doi:10.1111/j.1365-3121.2011.01005.x
- Mattinson, J.M. (2005): Zircon U-Pb chemical abrasion ("CA-TIMS") method: combined annealing and multi-step partial dissolution analysis for improved precision and accuracy of zircon ages. *Chemical Geology* 220, 47-66. doi:10.1016/j.chemgeo.2005.03.011
- McDonough, W.F., Sun, S. (1995): The composition of the Earth. *Chemical Geology* 120, 223-253. doi:10.1016/0009-2541(94)00140-4
- Miller, C.F., McDowell, S.M., Mapes, R.W. (2003): Hot and cold granites? Implications of zircon saturation temperatures and preservation of inheritance. *Geology* 31, 529-532. doi:10.1130/0091-7613(2003)031<0529:HACGIO>2.0.CO;2
- Neiva, A., Teixeira, R., Lima, S., Silva, P. (2013): *Idade, origem e protólitos de granitos Variscos de três áreas portuguesas*. Memorias da Academia das Ciências de Lisboa, Classe Ciências, Lisboa, 13 p.
- Neiva, A.M.R., Williams, I.S., Ramos, J.M.F., Gomes, M.E.P., Silva, M.M.V.G., Antunes, I.M.H.R. (2009): Geochemical and isotopic constraints on the petrogenesis of Early Ordovician granodiorite and Variscan two-mica granites from the Gouveia area, central Portugal. *Lithos* 111, 186-202. doi:10.1016/j.lithos.2009.01.005
- Orejana, D., Villaseca, C., Armstrong, R.A., Jeffries, T.E. (2011): Geochronology and trace element chemistry of zircon and garnet from granulite xenoliths: constraints on the tectonothermal evolution of the lower crust under central Spain. *Lithos* 124, 103-116. doi:10.1016/j.lithos.2010.10.011
- Orejana, D., Villaseca, C., Valverde-Vaquero, P., Belousova, E.A., Armstrong, R.A. (2012): U-Pb geochronology and zircon composition of late Variscan S-and I-type granitoids from the Spanish Central System batholith. *International Journal of Earth Sciences* 101, 1789-1815. doi: 10.1007/s00531-012-0750-y
- Pereira, M. F., Linnemann, U., Hofmann, M., Chichorro, M., Solá, A. R., Medina, J., Silva, J. B. (2012): The provenance of Late Ediacaran and Early Ordovician siliciclastic rocks in the Southwest Central Iberian Zone: Constraints from detrital zircon data on northern Gondwana margin evolution during the late Neoproterozoic. *Precambrian Research* 192, 166-189. doi:10.1016/j.precamres.2011.10.019
- Pérez-Soba, C., Villaseca, C., Del Tánago, J.G., Nasdala, L. (2007): The composition of zircon in the peraluminous Hercynian granites of the Spanish Central System batholith. *The Canadian Mineralogist* 45, 509-527. doi:10.2113/gscannmin.45.3.509
- Pupin, J.-P. (2000): Granite genesis related to geodynamics from Hf-Y in zircon. *Transactions-Royal Society of Edinburgh* 91, 245-256. doi:10.1130/0-8137-2350-7.245
- Quesada C., Florido, P., Gumi, P., Osborne, J. (1987): *Mapa Geológico-Minero de Extremadura E. 1:300.000*. Junta de Extremadura.
- Ramirez, J., Menéndez, L. (1999): A geochemical study of two peraluminous granites from south-central Iberia; the Nisa-Albuquerque and Jalama batholiths. *Mineralogical Magazine* 63, 85-104. doi:10.1180/002646199548330
- Recio, C., Fallick, A., Ugidos, J. (1992): A stable isotopic ( $\delta^{18}\text{O}$ ,  $\delta\text{D}$ ) study of late Hercynian granites and their host-rocks in the Central

- Iberian Massif (Spain). *Transactions-Royal Society of Edinburgh* 83, 247-257. doi:10.1017/S0263593300007938
- Rodríguez, L.R., López, F., Martín, J., Rubio, F. (2008): *Mapa Geológico de la Península Ibérica, Baleares y Canarias E. 1:1.000.000.* I.G.M.E., Madrid.
- Rodríguez-Alonso, M.D., Peinado, M., López-Plaza, M., Franco, P., Carnicer, A., Gonzalo, J.C. (2004): Neoproterozoic–Cambrian synsedimentary magmatism in the Central Iberian Zone (Spain): geology, petrology and geodynamic significance. *International Journal of Earth Sciences* 93, 897-920. doi:10.1007/s00531-004-0425-4
- Rodríguez-Pevida L, Mira, M., Ortega E. (1990): Hoja geológica num. 833 (Espiel). *Mapa Geológico de España E. 1:50.000.* I.G.M.E., Madrid.
- Rubio-Ordóñez, A., Valverde-Vaquero, P., Corretgé, L.G., Cuesta-Fernández, A., Gallastegui, G., Fernández-González, M., Gerdes, A. (2012): An Early Ordovician tonalitic–granodioritic belt along the Schistose-Greywacke domain of the Central Iberian zone (Iberian Massif, Variscan belt). *Geological Magazine* 149, 927. doi:10.1017/S0016756811001129
- Ruiz, C., Fernández-Leyva, C., Locutura, J. (2008): Geochemistry, geochronology and mineralisation potential of the granites in the Central Iberian Zone: the Jálama Batholith. *Chemie der Erde-Geochemistry* 68, 413-429. doi:10.1016/j.chemer.2006.11.001
- Scherer, E., Münker, C., Mezger, K. (2001): Calibration of the lutetium-hafnium clock. *Science* 293, 683-687. doi:10.1126/science.1061372
- Söderlund, U., Johansson, L. (2002): A simple way to extract baddeleyite ( $ZrO_2$ ). *Geochemistry Geophysics Geosystems* 3, 1-7. doi:10.1029/2001GC000212
- Solá, A.R., Pereira, M.F., Williams, I.S., Ribeiro, M.L., Neiva, A.M.R., Bea, F., Zinger, T. (2008): New insights from U-Pb zircon dating of Early Ordovician magmatism on the northern Gondwana margin: The Urria Formation (SW Iberian Massif, Portugal). *Tectonophysics* 461, 114-129. doi:10.1016/j.tecto.2008.01.011
- Solá, A.R., Williams, I.S., Neiva, A.M., Ribeiro, M.L. (2009): U-Th-Pb SHRIMP ages and oxygen isotope composition of zircon from two contrasting late Variscan granitoids, Nisa-Albuquerque batholith, SW Iberian Massif: Petrologic and regional implications. *Lithos* 111, 156-167. doi:10.1016/j.lithos.2009.03.045
- Speer, J.A. (1982): Zircon. In: P.H. Ribbe (ed.), *Orthosilicates. Reviews in Mineralogy and Geochemistry* 5, Mineralogical Society of America, Virginia, pp. 67-112.
- Stacey, J.T., Kramers, J. (1975): Approximation of terrestrial lead isotope evolution by a two-stage model. *Earth and Planetary Science Letters* 26, 207-221. doi:10.1016/0012-821X(75)90088-6
- Talavera, C., Montero, P., Martínez Poyatos, D., Williams, I. (2012): Ediacaran to Lower Ordovician age for rocks ascribed to the Schist-Graywacke Complex (Iberian Massif, Spain): Evidence from detrital zircon SHRIMP U-Pb geochronology. *Gondwana Research* 22, 928-942. doi:10.1016/j.gr.2012.03.008
- Tartèse, R., Boulvais, P. (2010): Differentiation of peraluminous leucogranites “en route” to the surface. *Lithos* 114, 353-368. doi:10.1016/j.lithos.2009.09.011
- Taylor, H.P. (1978): Oxygen and hydrogen isotope studies of plutonic granitic rocks. *Earth and Planetary Science Letters* 38, 177-210. doi:10.1016/0012-821X(78)90131-0
- Teixeira, R.J.S., Neiva, A.M.R., Silva, P.B., Gomes, M.E.P., Andersen, T., Ramos, J.M.F. (2011): Combined U-Pb geochronology and Lu-Hf isotope systematics by LAM-ICPMS of zircons from granites and metasedimentary rocks of Carrazeda de Ansiães and Sabugal areas, Portugal, to constrain granite sources. *Lithos* 125, 321-334. doi:10.1016/j.lithos.2011.02.015
- Ugidos, J., Valladares, M.I., Recio, C., Rogers, G., Fallick, A.E., Stephens, W.E. (1997): Provenance of Upper Precambrian-Lower Cambrian shales in the Central Iberian Zone, Spain: evidence from a chemical and isotopic study. *Chemical Geology* 136, 55-70. doi:10.1016/S0009-2541(96)00138-6
- Valle Aguado, B., Azevedo, M.R., Schaltegger, U., Martínez Catalán, J.R., Nolan, J. (2005): U-Pb zircon and monazite geochronology of Variscan magmatism related to syn-convergence extension in Central Northern Portugal. *Lithos* 82, 169-184. doi:10.1016/j.lithos.2004.12.012
- Villaseca, C., Barbero, L., Rogers, G. (1998): Crustal origin of Hercynian peraluminous granitic batholiths of Central Spain: petrological, geochemical and isotopic (Sr, Nd) constraints. *Lithos* 43, 55-79. doi:10.1016/S0024-4937(98)00002-4
- Villaseca, C., Belousova, E., Orejana, D., Castiñeiras, P., Pérez-Soba, C. (2011): Presence of Palaeoproterozoic and Archean components in the granulite-facies rocks of central Iberia: The Hf isotopic evidence. *Precambrian Research* 187, 143-154. doi:10.1016/j.precamres.2011.03.001
- Villaseca, C., Herreros, V. (2000): A sustained felsic magmatic system: the Hercynian granitic batholith of the Spanish Central System. *Transactions of the Royal Society of Edinburgh* 91, 207-219. doi:10.1017/S0263593300007380
- Villaseca, C., Merino, E.; Oyarzun R.; Orejana, D.; Pérez-Soba, C.; Chicharro E. (2014): Contrasting chemical and isotopic signatures from Neoproterozoic metasedimentary rocks in the Central Iberian Zone (Spain) of pre-Variscan Europe: Implications for terrane analysis and Early Ordovician magmatic belts. *Precambrian Research* 245, 131-145. doi:10.1016/j.precamres.2014.02.006
- Villaseca, C., Orejana, D., Belousova, E.A. (2012): Recycled metaigneous crustal sources for S-and I-type Variscan granitoids from the Spanish Central System batholith: Constraints from Hf isotope zircon composition. *Lithos* 153, 84-93. doi:10.1016/j.lithos.2012.03.024
- Villaseca C., Pérez-Soba C., Merino E., Orejana D., López-García J.A., Billstrom K. (2008): Contrasted crustal sources for peraluminous granites of the segmented Montes de Toledo Batholith (Iberian Variscan Belt). *Journal of Geosciences* 53, 263-280. doi:10.3190/jgeoisci.035
- Vindel, E., Chicharro, E., Villaseca, C., López-García, J.A., Sánchez, V. (2014): Hydrothermal phosphate vein-type ores from the southern Central Iberian Zone, Spain: Evidences for their relationship to granites and Neoproterozoic metasedimentary rocks. *Ore Geology Reviews* (In Press, Accepted). doi:10.1016/j.oregeorev.2014.03.011
- Wang, X., Griffin, W., Chen, J. (2010): Hf contents and Zr/Hf ratios in granitic zircons. *Geochemical Journal* 44, 65-72.
- Watson, E.B., Harrison, T.M. (1983): Zircon saturation revisited: temperature and composition effects in a variety of crustal magma types. *Earth and Planetary Science Letters* 64, 295-304. doi:10.1016/0012-821X(83)90211-X
- Watson, E.B., Harrison, T.M. (2005): Zircon Thermometer Reveals Minimum Melting Conditions on Earliest Earth. *Science* 308, 841-844. doi:10.1126/science.1110873
- Wiedenbeck, M., Allé, P., Corfu, F., Griffin, W.L., Meier, M., Oberli, F., von Quadt, A., Roddick, J.C., Spiegel, W. (1995): Three natural zircon standards for U-Th-Pb, Lu-Hf, trace element and REE analyses. *Geostandards Newsletter* 19, 1-23. doi:10.1111/j.1751-908X.1995.tb00147.x
- Woodhead, J.D., Hergt, J.M. (2005): A preliminary appraisal of seven natural zircon reference materials for in situ Hf isotope determination. *Geostandards and Geoanalytical Research* 29, 183-195. doi:10.1111/j.1751-908X.2005.tb00891.x
- Zeck, H., Wingate, M., Pooley, G. (2007): Ion microprobe U-Pb zircon geochronology of a late tectonic granitic–gabbroic rock complex within the Hercynian Iberian belt. *Geological Magazine* 144, 157-177. doi:10.1017/S0016756806002652